Referee's Comment in Italic Font; **Author's response in Red** **and Manuscript revision in Blue without Italic Font.**

This manuscript by Li et al. describes observations of structural impact on SOA formation from C8-C9 aromatic hydrocarbons in chamber studies. This work provides comprehensive dataset of SOA formation, including SOA yield data, elemental chemical composition data from AMS, and SOA density and volatility data. Although SOA formation from aromatic hydrocarbons has been studied for over 20 years (as the authors cited), the insights from the analyses using new techniques and new knowledge are beyond the level that scientists had discovered 20 years ago. Thus I think this manuscript is appropriate to be published in ACP. In the revised manuscript, the authors have addressed most of the comments from previous reviewers, but some small issues still need to be addressed, mostly related to the SOA yield part:

1. It might be misleading to use the term "low NOx" to describe the experimental conditions. 20-140 ppb of NO is relatively "low NOx" in chamber studies, but not the same case for ambient conditions. This point was also raised by Reviewer #2. I think what really matters is not the NOx level, but the relative branching ratios of different RO2 reaction pathways (RO2 + NO vs. RO2 + HO2 vs. RO2 + RO2), which can be simulated/estimated using SAPRC. For example, in experiment 1226B and 1421A, with very distinct NO levels, if the authors provide a simulation result (in main paper or supplemental information) to show that under such a range of NO levels, RO2 + HO2 is always the dominant pathway (e.g., >70% in these experiments), then I think the argument about the NOx level is clarified.

It is a good suggestion. The following graphs are added into supporting information as Fig. S1 to show that under such a range of NO levels, $RO_2 + HO_2$ is always the dominant pathway (e.g., >70% in these experiments)
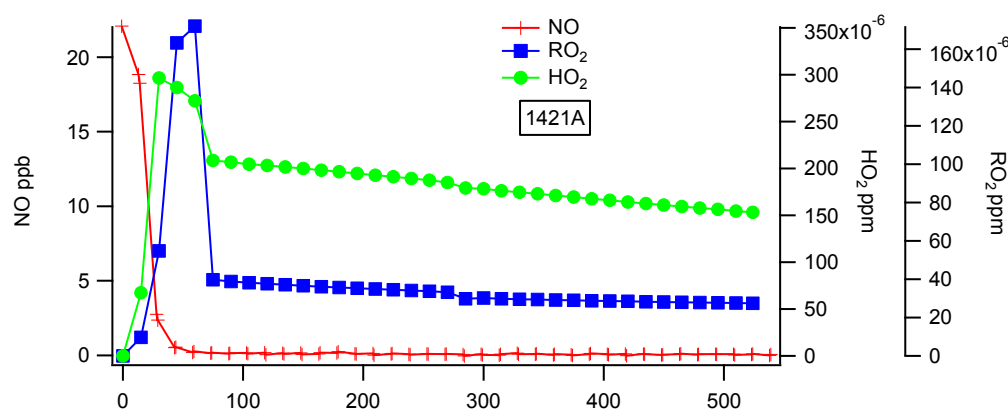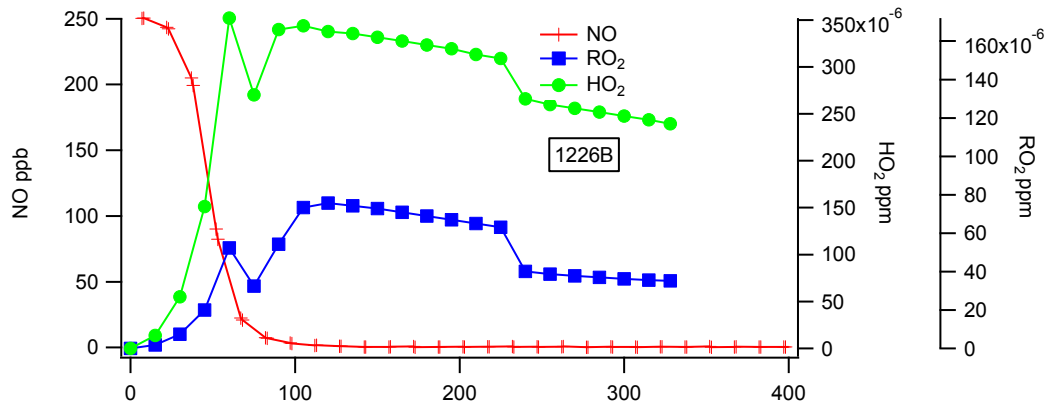
2. It is also useful to provide AMS mass spectra comparison of SOA from the same aromatic hydrocarbon under different HC:NOx conditions. How much change occurred to SOA chemical composition when initial HC:NOx condition changed? Without clarification of these changes, it is difficult to argue that the SOA yield difference is mainly due to different molecular structure, not different products under various experimental conditions.

The average AMS mass spectra of SOA formation from *o*-xylene under different initial NO [50 ppb NO+ 80 ppb o-xylene (1320A) and 20ppb NO + 80ppb *o*-xylene (repeat experiment of 1321A) is provided in the graph below. We also compare the difference of SOA formed under different NO conditions in f_{44} vs f_{43} and H/C vs O/C graphs. There is no significant chemical composition difference observed in SOA formed under different NO conditions.
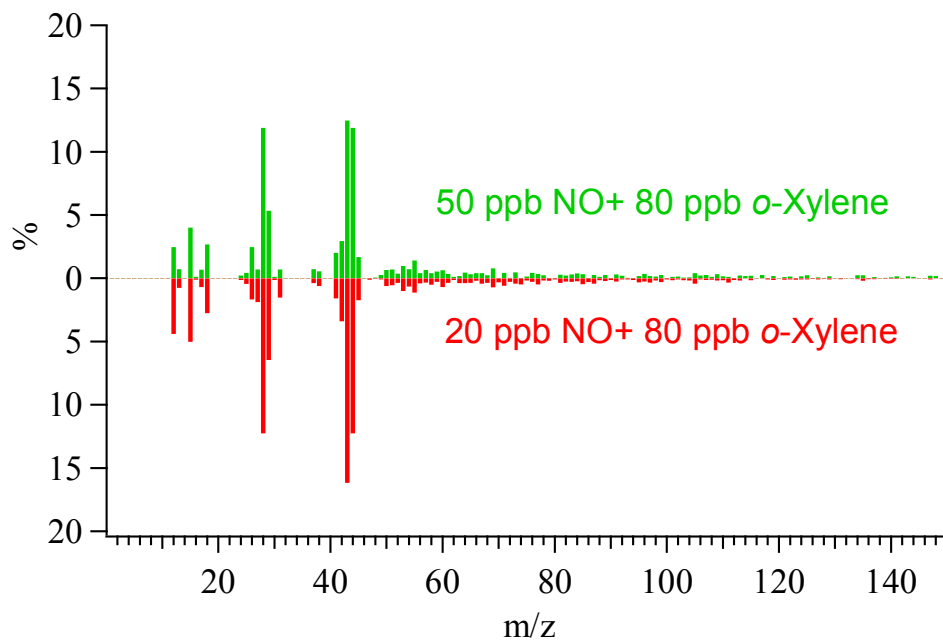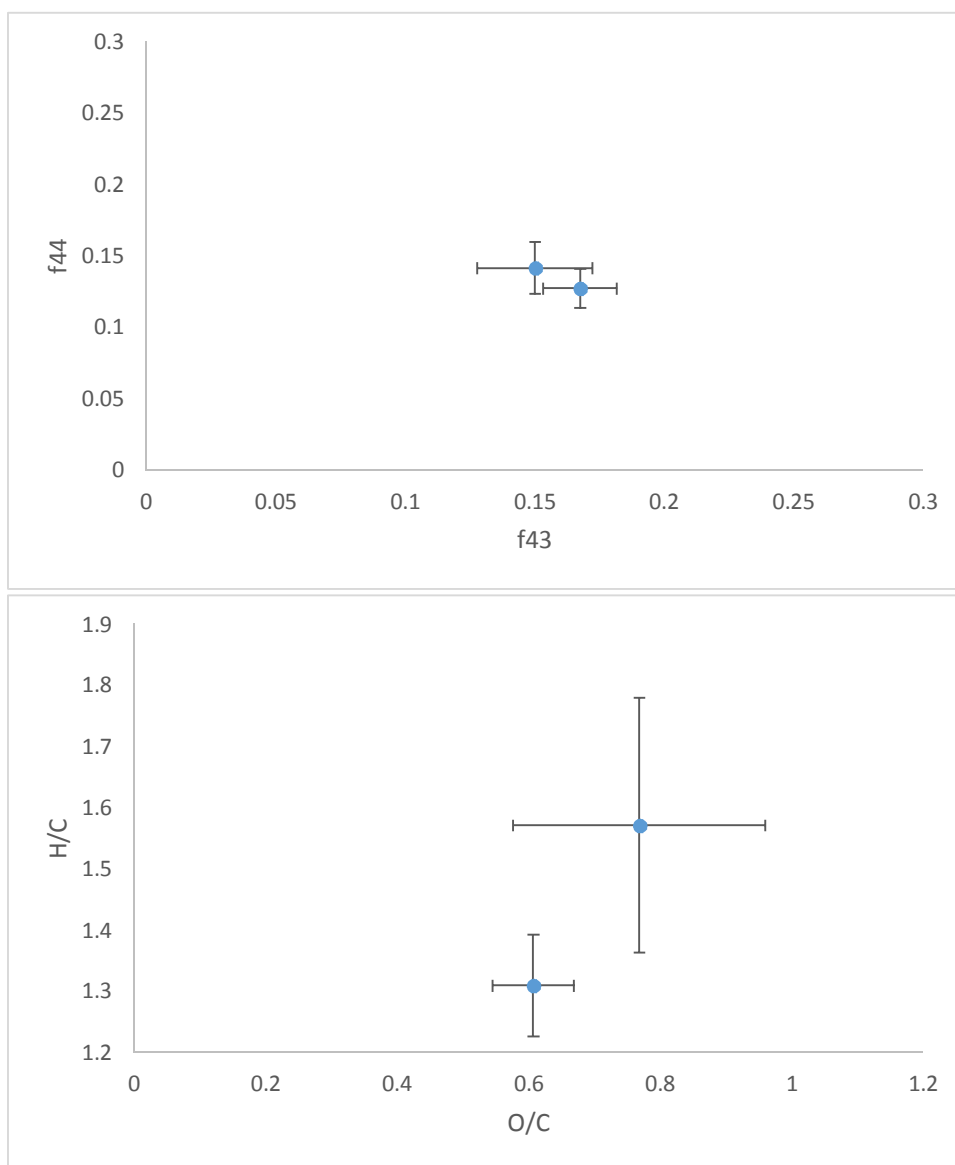
3. The authors claimed that ortho position substituted aromatic hydrocarbons have highest SOA yield, based on observations. I think the authors should add some more discussion and provide some mechanistic insights to explain these observations, combining with the AMS chemical composition data. The discussion in Section 5, from line 14 is helpful to understand the observation, but need to re-organize and extend to a separate section with chemical structure schemes, if possible. For example, are ortho position substituted aromatic hydrocarbon products less likely to fragment due to the structure?

Thanks reviewer for the suggestion. We discuss about the promoting of SOA formation by the ortho position in Section from line 14 to Line 25 by suggesting the different mechanism associated with different molecular structure (ortho, para and meta). We would like to add more discussion on that if we could. However, our study is based on the bulk chemical composition measured on AMS. We do not have enough information to make a justifiable discussion. Further study on the speciation of SOA components is suggested to improve the understanding of SOA formation mechanism from different isomer.

The Figure numbers used in the manuscript are modified accordingly since a new Fig. S1 is added as a response to the first comment of reviewer #4.

Impact of Molecular Structure on Secondary Organic Aerosol Formation from Aromatic Hydrocarbon Photooxidation under Low NO$_X$ Conditions

L. Li[1,2], P. Tang[1,2], S. Nakao[1,2,3] and D. R. Cocker III[1,2]

[1] University of California, Riverside, Department of Chemical and Environmental Engineering, Riverside, CA 92507, USA

[2] College of Engineering-Center for Environmental Research and Technology (CE-CERT), Riverside, CA 92507, USA

[3] Currently at Clarkson University, Department of Chemical and Biomolecular Engineering, Potsdam, NY 13699, USA

Correspondence to: D. Cocker III (dcocker@engr.ucr.edu)

Abstract

The molecular structure of volatile organic compounds (VOC) determines their oxidation pathway, directly impacting secondary organic aerosol (SOA) formation. This study comprehensively investigates the impact of molecular structure on SOA formation from the photooxidation of twelve different eight- to nine-carbon aromatic hydrocarbons under low NO$_x$ conditions. The effects of the alkyl substitute number, location, carbon chain length and branching structure on the photooxidation of aromatic hydrocarbons are demonstrated by analyzing SOA yield, chemical composition and physical properties. Aromatic hydrocarbons, categorized into five groups, show a yield order of ortho (*o*-xylene and *o*-ethyltoluene)> one substitute (ethylbenzene, propylbenzene and isopropylbenzene) > meta (*m*-xylene and *m*-ethyltoluene)> three substitute (trimethylbenzenes) > para (*p*-xylene and *p*-ethyltoluene). SOA yields of aromatic hydrocarbon photooxidation do not monotonically decrease when increasing alkyl substitute number. The ortho position promotes SOA formation while the para position suppresses aromatic oxidation and SOA formation. Observed SOA chemical

composition and volatility confirm that higher yield is associated with further oxidation. SOA chemical composition also suggests that aromatic oxidation increases with increasing alkyl substitute chain length and branching structure. Further, carbon dilution conjecture developed by Li., et al (2016) is extended in this study to serve as a standard method to determine the

5   extent of oxidation of an alkyl substituted aromatic hydrocarbon.

Key Words

Secondary Organic Aerosol; Aromatic Hydrocarbon; Molecular Structure; Alkyl Substitute; SOA Yield; Chemical Composition; Volatility

1. Introduction

10   Organic aerosols are critical to human health (Dockery, et al., 1993; Krewski, et al., 2003; Davidson et al., 2005), climate change (IPCC, 2007) and visibility (Pöschl 2005; Seinfeld and Pandis, et al., 2006). Global anthropogenic secondary organic aerosol (SOA) sources are underestimated by current models (Henze, et al., 2008; Matsui, et al., 2009; Hallquist, et al., 2009; Farina, et al., 2010) and are more likely to increase due to the increase of known

15   anthropogenic emissions (Heald, et al., 2008). Therefore, it is crucial to explore SOA formation mechanism from anthropogenic precursors.

Aromatic hydrocarbons are major anthropogenic SOA precursors (Kanakidou, et al., 2005; Henze, et al., 2008; Derwent, et al., 2010). C_8 (ethylbenzene, xylenes) and C_9 (ethyltoluenes and trimethylbenzenes) aromatics are important aromatic hydrocarbons in the atmosphere

20   besides toluene and benzene (Monod, et al., 2001; Millet, et al., 2005; Heald, et al., 2008; Kansal, et al., 2009; Hu, et al., 2015). The major sources of C_8 and C_9 aromatic hydrocarbons are fuel evaporation (Kaiser, et al., 1992; Rubin, et al., 2006; Miracolo, et al., 2012), tailpipe exhaust (Singh, et al, 1985; Monod, et al., 2001; Lough, et al., 2005; Na, et al., 2005; Correa and Arbilla, et al., 2006) and solvent use (Zhang, et al., 2013). C_8 aromatic hydrocarbons

25   (ethylbenzene and xylenes (ortho, meta and para) are categorized as hazardous air pollutants (HAPs) under the US Clean Air Act Amendments of 1990

(http://www.epa.gov/ttnatw01/orig189.html)). Toluene and C_8 aromatics dominate the anthropogenic SOA precursors and SOA yield from all C_9 aromatics is currently predicted to be equal to that of toluene (Bahreini, et al., 2009). The chemical composition of aromatic SOA remains poorly understood with less than 50% of aromatic hydrocarbon photooxidation

5   products identified (Forstner, et al., 1997; Fisseha, et al., 2004; Hamilton et al., 2005; Sato et al., 2007). Aromatic hydrocarbon photooxidation mechanisms remain uncertain except for the initial step (~90% OH-addition reaction) (Calvert, et al., 2002). Hence, understanding the atmospheric reaction mechanisms of C_8 and C_9 aromatic hydrocarbons and properly quantifying their SOA formation potential presents unique challenges due to the variety in

10   their molecular structure and the electron density of the aromatic ring.

Volatile organic compound (VOC) structure impacts the gas phase reaction mechanism (Ziemman and Atkinson, 2012) and kinetic reaction rate (eg. k_{OH} Atkinson, 1987) thereby influencing the resulting SOA properties and mass yield. Molecular structure impacts on SOA formation from alkanes have been previously studied (Lim and Ziemann, 2009; Ziemann,

15   2011; Lambe, et al., 2012; Tkacik, et al., 2012; Yee, et al., 2013; Loza, et al., 2014). It is generally observed that SOA yield decreases from cyclic alkanes to linear alkanes and to branched alkanes. The relative location of the methyl group on the carbon chain also affects SOA yield (Tkacik, et al., 2012). It is further found that the SOA yield and structure relationship is influenced by C=C groups (Ziemann, 2011). Understanding the SOA yield and

20   structure relationship of aromatic compounds in a similar way is necessary due to the atmospheric importance of aromatic hydrocarbons.

Previously, aromatic studies categorized SOA yield solely based on substitute number (Odum, 1997a, b). However, those chamber experiments were conducted at high NO_x conditions, which are well above levels present in the atmosphere. Song, et al (2005, 2007) found that

25   initial HC/NO_x ratios significantly impact SOA yields during aromatic photooxidation with yields increasing as NO_x levels decreased. Ng et al. (2007) shows there is no significant yield difference between one substitute (toluene) and two substitute (*m*-xylene) aromatics in the absence of NO_x. The current work focuses on molecular structure impact on SOA formation at more atmospherically relevant NO_x and aerosol loadings. Li et al (2016) demonstrated the

methyl group number impact on SOA formation under low NO_x conditions. Also, aromatic compounds with para position alkyl groups have been observed to form less SOA under various NO_x conditions than their isomers in previous studies. Izumi and Fukuyama (1990) found that *p*-xylene, *p*-ethyltoluene and 1, 2, 4-trimethylbenzene have low SOA formation

5   potential under high NO_x conditions. Song, et al (2007) observed that *p*-xylene has the smallest SOA yield among all xylenes in the presence of NO_x. The relative methyl position to -OH in dimethyl phenols also impacts SOA yield in the absence of NO_x (Nakao, et al., 2011), while Song et al.(2007) observed no significant SOA yield difference between *o*-xylene and *p*-xylene under NO_x free conditions. Moreover, previous studies mainly focused on the carbon

10   number effect on SOA formation (Lim and Ziemann, 2009; Li, et al, 2016) and seldom addressed the substitute carbon length impact on VOC oxidation and hence SOA formation. Different percentages of similar compounds are found when the substitute carbon length on the aromatic ring changes (Forstner, et al., 1997; Huang, et al., 2007; Huang, et al., 2011). For example, a lower percentage of 3-methyl-2, 5-furanone is observed in toluene than that of

15   3-ethyl-2, 5-furanone in ethylbenzene (Forstner, et al., 1997). Further, the branching structure on the aromatic substitute might impact the reaction pathway. It is possible that fragmentation is more favored on branched substitute alkoxy radicals than n-alkane substituents similar to alkanes (Atkinson, et al., 2003).

Few studies comprehensively consider the overall alkyl effect on SOA formation from

20   aromatic hydrocarbons, including the substitute number, position, carbon chain length and branching structure, especially under low NO_x conditions. It is valuable to understand the relationship between aromatic hydrocarbon molecular structures and SOA physical and chemical characteristics. The effects of OH exposure (Lambe, et al., 2011 (alkane), 2015), mass loading (Shilling, et al., 2009 (α-pinene); Pfaffenberger, et al., 2013(α-pinene)) and NO

25   condition (Ng, et al., 2007; Eddingsaas, et al., 2012(α-pinene)) on SOA physical and chemical characteristics are previously discussed. However, few studies address the molecular structure effect of the precursor on SOA chemical composition, especially under atmospherically relevant conditions. Sato et al (2012) shows the chemical composition difference between ethylbenzene, *m*-xylene, *o*-xylene, 1, 2, 4-trimethylbenzene and 1, 3,

5-trimethylbenzene under high absolute NO_x conditions and hypothesizes that ketones prevent further oxidation during aromatic photooxidation compared with aldehydes. The SOA products detected in Sato's study are mainly small volatile compounds which are less likely to partition into the particle phase (Chhabra, et al., 2011). Therefore, the study of Sato, et al.

5   (2012) indicates that further oxidation or oligmerization might contribute to SOA formation during aromatic photooxidation. Less SOA characterization data on propylbenzene and ethyltoluene compared with trimethylbenzene is available. However, Bahreini, et al. (2009) suggests that the sum of the propylbenzene and ethyltoluene is on average a factor of 4–10 more abundant than trimethylbenzene.

10   This work examines twelve aromatic hydrocarbons, all of which are isomers with eight or nine carbons, to investigate the impact of molecular structure on SOA formation from aromatic hydrocarbon photooxidation under low NO_x (10-138 ppb). Here, we investigate the substitute number, substitute position, alkyl carbon chain length and alkyl branching impacts on aromatic hydrocarbon oxidation. The effects of molecular structure impact on SOA yield,

15   chemical composition (H/C, O/C, OS_c, f_{44}, f_{43}, f_{57} and f_{71}) and physical properties (density and VFR) are demonstrated. Alkyl substitute dilution conjecture is further developed from methyl dilution theory (Li, et al., 2016).

2. Method

2.1 Environmental chamber

20   The UC Riverside/CE-CERT indoor dual 90 m^3 environmental chambers were used in this study and are described in detail elsewhere (Carter et al., 2005). Experiments were all conducted at dry conditions (RH<0.1%), in the absence of inorganic seed aerosol and with temperature controlled to 27±1°C. Seeded experiments to minimize wall effects have also been conducted in our chamber experiment with no measurable difference observed between

25   the seeded and non-seeded experiment. Two movable top frames were slowly lowered during each experiment to maintain a slight positive differential pressure (~0.02" H_2O) between the

reactors and enclosure to minimize dilution and/or contamination of the reactors. 272 115 W

Sylvania 350BL blacklights are used as light sources for photooxidation.

A known volume of high purity liquid hydrocarbon precursors (ethylbenzene Sigma-Aldrich,

99.8%; n-propylbenzene Sigma-Aldrich, 99.8%; isopropylbenzene Sigma-Aldrich, analytical

5   standard; *m*-xylene Sigma-Aldrich, 99%; *o*-xylene Sigma-Aldrich, 99%; *p*-xylene

Sigma-Aldrich, 99%; *m*-ethyltoluene Sigma-Aldrich, 99%; *o*-ethyltoluene Sigma-Aldrich,

99%; *p*-ethyltoluene Sigma-Aldrich, ≥95%; 1, 2, 3-trimethylbenzene Sigma-Aldrich,

OEKANAL analytical standard; 1, 2, 4-trimethylbenzene Sigma-Aldrich, 98%; 1, 3,

5-trimethylbenzene Sigma-Aldrich, analytical standard) was injected through a heated glass

10   injection manifold system and flushed into the chamber with pure N_2. NO was introduced by

flushing pure N_2 through a calibrated glass bulb filled to a predetermined partial pressure of

pure NO. All hydrocarbons and NO are injected and well mixed before lights are turned on to

start the experiment.

2.2 Particle and Gas Measurement

15   Particle size distribution between 27 nm and 686 nm was monitored by dual custom built

Scanning Mobility Particle Sizers (SMPS) (Cocker et al., 2001). Particle effective density was

measured with an Aerosol Particle Mass Analyzer (APM-SMPS) system (Malloy et al., 2009).

Particle volatility was measured by a Dekati® Thermodenuder Volatility Tandem Differential

Mobility Analyzer (VTDMA) (Rader and McMurry, 1986) with a 17 s heating zone residence

20   time (Qi, et al., 2010a). The heating zone was controlled to 100 °C in this study with Volume

Fraction Remaining (VFR) calculated as $(D_{p, \text{ after TD}}/D_{p, \text{ before TD}})^3$.

Particle-phase chemical composition evolution was measured by a High Resolution Time of

Flight Aerosol Mass Spectrometer (HR-ToF-AMS; Aerodyne Research Inc.) (Canagaratna et

al., 2007; DeCarlo et al., 2006). The sample was vaporized by a 600 °C oven under vacuum

25   followed by a 70 eV electron impact ionization. f_x in this study is calculated as the mass

fraction of the organic signal at *m/z*=x. For example, f_{44}, f_{43}, f_{57} and f_{71} are the ratios of the

organic signal at *m/z* 44, 43, 57 and 71 to the total organic signal, respectively (Chhabra et al.,

2011; Duplissy et al., 2011). Elemental ratios for total organic mass, oxygen to carbon (O/C),

and hydrogen to carbon (H/C) were determined using the elemental analysis (EA) technique (Aiken et al., 2007, 2008). Data was analyzed with ToF-AMS analysis toolkit Squirrel 1.56D /Pika 1.15D version. Evolution of SOA composition (Heald, et al., 2010; Jimenez, et al., 2009) refers to SOA chemical composition changes with time. f_{44} and $f_{43+57+71}$ evolution and H/C and O/C evolution refer to the change of f_{44} and $f_{43+57+71}$ with time and the change of H/C and O/C with time, respectively.

The Agilent 6890 Gas Chromatograph – Flame Ionization Detector was used to measure aromatic hydrocarbon concentrations. A Thermal Environmental Instruments Model 42C chemiluminescence NO analyzer was used to monitor NO, NO_y-NO and NO_y. The gas-phase reaction model SAPRC-11 developed by Carter and Heo (2013) was utilized to predict radical concentrations ($\cdot OH$, $HO_2\cdot$, $RO_2\cdot$ and $NO_3\cdot$).

3. Result

3.1 SOA yield

Photooxidation of twelve C_8 and C_9 aromatic hydrocarbons were studied for low NO_x conditions (HC/NO ratio 11.1-171 ppbC:ppb). SOA yields for all aromatic hydrocarbons were calculated according to Odum, et al. (1996) as the mass ratio of aerosol formed to parent hydrocarbon reacted. Experimental conditions and SOA yields are listed (Table.1) along with additional *m*-xylene, *o*-xylene, *p*-xylene and 1, 2, 4-trimethylbenzene experimental conditions from previous studies (Song, et al, 2005; Song, et al, 2007; Li, et al, 2016) (Table S2). The uncertainty associated with 10 replicate *m*-xylene and NO experiments SOA yield is <6.65%. SOA yield as a function of particle mass concentration (M_o), shown in Fig. 1, includes experiments listed in both Table 1 and Table S2. It is observed that both alkyl substitute number and position affect SOA yield. The SOA yield of two-substitute C_8 and C_9 aromatic hydrocarbons depends more on the substitute location than substitute length. This means that the yield trend of *o*-xylene is analogous to that of *o*-ethyltoluene. Similarly, the yield trends for meta and para position substituted C_8 and C_9 aromatic hydrocarbons will be analogous to each other. Ortho isomers (*o*-xylene and *o*-ethyltoluene, marked as solid and hollow green

circles, respectively) have the highest SOA yield for similar aerosol concentrations while para isomers (*p*-xylene and *p*-ethyltoluene, marked as solid and hallow blue diamonds, respectively) have the lowest SOA yield level. Lower SOA yield for para isomers are consistent with previous observation by Izumi and Fukuyama (1990). Izumi and Fukuyama

5 (1990) also suggest that 1, 2, 4-trimethylbenzene yields are lower than for other aromatic hydrocarbons. The current study does not show a significant SOA yield difference between 1, 2, 4-trimethylbenzene and 1, 3, 5-trimethylbenzene. It is difficult to compare 1, 2, 3-trimethylbenzene yields with the former two trimethylbenzenes since 1, 2, 3-trimethylbenzene mass loading is much higher than the former two.

10 Aromatic hydrocarbons having only one substitute (ethylbenzene, n-propylbenzene and isopropylbenzene) or three substitutes (1, 2, 3-trimethylbenzene, 1, 2, 4-trimethylbenzene and 1, 3, 5-trimethylbenzene) tend to have yields similar to the meta position two alkyl aromatics. Odum, et al (1997b) categorized SOA yield formation potential solely based on substitute number and stated that aromatics with less than two methyl or ethyl substitutes form more

15 particulate matter than those with two or more methyl or ethyl substitutes on the aromatic ring. However, Odum's work was conducted for high NO_x conditions and had insufficient data to compare isomer yield differences (e.g., only two low mass loadings for *o*-xylene data). The strong low yield (two or more substitutes) and high yield (less than two methyl or ethyl substitutes) trends for high NO_x conditions (Odum, et al., 1997) are not observed for low NO_x

20 aromatic experiments in this study. Rather, high yield is observed only for benzene (Li, et al., 2016) while low yield is seen for substituted aromatic hydrocarbons. Similar SOA yield trends from different C_8 and C_9 aromatic isomers are further confirmed by comparing yields at similar radical conditions (Table S4, Fig. ~~S2~~S3). It is also found that molecular structure exerts a greater impact on SOA yield than reaction kinetics (supplemental material, Table S5).

25 A two product model described by Odum, et al. (1996) is used to fit SOA yield curves as a function of M_o. The twelve aromatics are categorized into five groups to demonstrate the alkyl group number and position effect on SOA formation. The five groups include one substitute group (1S), ortho position two alkyl group (ortho), meta position two alkyl group (meta), para position two alkyl group (para) and three substitute group (3S). Fitting parameters (α_1, $K_{om,1}$,

α_2 and $K_{om,2}$; Table 2) in the two product model are determined by minimizing the sum of the squared residuals. The lower volatility partitioning parameter ($K_{om,2}$) is the same for all yield curve fits by assuming similar high volatile compounds are formed during all aromatic hydrocarbon photooxidation experiments. The ortho group is associated with a much higher

5    $K_{om,1}$ compared with other aromatic groups, indicating aromatic hydrocarbon oxidation with an ortho position substitute forms much lower volatility products than other isomers. $K_{om,1}$ are also slightly higher in the meta group and one substitute groups than in the three substitute and para substitute groups.

A slight SOA yield difference remains within each group (Fig. ~~S1~~S2&Table. S3), indicating

10   the influence of factors other than alkyl group position. Generally, lower yields are found in aromatics with higher carbon number substitute alkyl groups, such as when comparing propylbenzene (i- and n-) with ethylbenzene or toluene (Li, et al., 2016), *m*-ethyltoluene with *m*-xylene and *p*-ethyltoluene with *p*-xylene, respectively. These differences are explained by the proposed alkyl group dilution effect (Section 4). However, the differences between

15   xylenes and their corresponding ethyltoluenes are not statistically significant.

3.2 Chemical composition

3.2.1 f_{44} vs $f_{43+57+71}$

The ratio of alkyl substitute carbon number (H:C >1) to the aromatic ring carbon number impacts SOA composition since the H:C ratio on the alkyl substitute is larger than 1 and the

20   H:C ratio on aromatic ring itself is no more than 1. m/z 43 ($C_2H_3O^+$ and $C_3H_7^+$) combined with m/z 44 (CO_2^+) are critical to characterize oxygenated compounds in organic aerosol (Ng, et al., 2010; Ng, et al., 2011). $C_2H_3O^+$ is the major contributor to m/z 43 in SOA formed from aromatic hydrocarbons having only methyl substitute (Li, et al., 2016) while $C_3H_7^+$ fragments are observed in this work for SOA from propylbenzene and isopropylbenzene (Fig. ~~S4~~S5,

25   Table S6). The $C_nH_{2n-1}O^+$ (n=carbon number of the alkyl substitute) fragment in SOA corresponds to a $C_nH_{2n+1}-$ alkyl substitute to the aromatic ring. $C_3H_5O^+$ (m/z 57) and $C_4H_7O^+$ (m/z 71) are important when investigating SOA from ethyl or propyl substitute aromatic

precursors. While m/z 57 ($C_4H_9^+$) and m/z 71 ($C_5H_{11}^+$) are often considered as markers for hydrocarbon-like organic aerosol in ambient studies (Zhang et al., 2015; Ng et al., 2010), oxygenated organic aerosol $C_3H_5O^+$and $C_4H_7O^+$ are the major fragments at m/z 57 and m/z 71, respectively, (Fig. ~~S4~~S5, Table S6) in current chamber SOA studies, especially during the photooxidation of ethyl and propyl substituted aromatics. Therefore, m/z 57 and m/z 71 are also considered beside $C_2H_3O^+$ at m/z 43 in SOA chamber studies as OOA to compare the oxidation of different aromatic hydrocarbons. Fig. ~~S4~~S5 lists all fragments found at *m/z* 43, 44, 57 and 71 and Fig. ~~S5~~S6 shows the fraction of each *m/z* in SOA formed from all aromatic hydrocarbons studied. The *m/z* 43+*m/z* 44+*m/z* 57+*m/z* 71 accounts for 21.2%~29.5% of the total mass fragments from all C_8 and C_9 aromatics studied, suggesting similar oxidation pathways. Only a small fraction (<~0.7%) of *m/z* 71 ($C_4H_7O^+$) or *m/z* 57 ($C_3H_5O^+$) was observed in ethyltoluenes and trimethylbenzenes, respectively.

This work extends the traditional f_{44} vs f_{43} ($C_2H_3O^+$) chemical composition analysis by including oxidized fragments ($C_3H_5O^+$ m/z 57 and $C_4H_7O^+$ m/z 71) of the longer (non-methyl) alkyl substitutes. Therefore, f_{44} vs $f_{43}+f_{57}+f_{71}$ is plotted instead of f_{44} vs f_{43}. Fig ~~S3~~S4 shows the evolution of f_{44} and $f_{43+57+71}$ in SOA formed from the photooxidation of different aromatic hydrocarbons at low NO_x conditions. f_{44} and $f_{43+57+71}$ ranges are comparable to previous chamber studies (Ng, et al., 2010; Chhabra, et al., 2011; Loza, et al., 2012; Sato, et al., 2012). Only slight f_{44} and $f_{43+57+71}$ evolution during chamber photooxidation is observed for the C_8 and C_9 isomers hence only the average f_{44} and $f_{43+57+71}$ will be analyzed in this work .

A modification is applied to the mass based *m/z* fraction in order to compare the mole relationship between *m/z* 44 and *m/z* 43+*m/z* 57+m/z 71(Eq-1).

$$f\,'_{43+57+71} = \frac{44}{43}f_{43} + \frac{44}{57}f_{57} + \frac{44}{71}f_{71}$$ Eq-1

The average f_{44} vs $f'_{43+57+71}$for all C_8 and C_9 isomers (Fig. 2) are located around the trend line for methyl group substituted aromatic hydrocarbons (Li, et al., 2016), implying a similarity in the SOA components formed from alkyl substituted aromatic hydrocarbons. A decreasing trend in oxidation from upper left to lower right is included in Fig 2, similar to what Ng, et al

(2011) found in the f_{44} vs f_{43} graph, especially while comparing similar structure compounds. The methyl group location on the aromatic ring impacts f_{44}: $f'_{43+57+71}$. Decreasing f_{44} and increasing $f'_{43+57+71}$ trends are observed from p-xylene to o-xylene to m-xylene and from 1, 2, 4-trimethylbenzene to 1, 2, 3-trimethylbenzene to 1, 3, 5-trimethylbenezene. The $f'_{43+57+71}$

5   may partially depend on the relative position between the alkyl substitute and the peroxide oxygen of the bicyclic peroxide. For instance, allylically stabilized five-membered bicyclic radicals are the most stable bicyclic radical formed from aromatic hydrocarbon photooxidation (Andino, et al., 1996). Two meta position substitutes connected to the aromatic ring carbon with -C-O- yield higher fractions of $C_nH_{2n-1}O^+$ fragments than the para

10   and ortho position, which have at most one substitute connected with -C-O- (Fig. ~~S6~~S7). CO_2^+ are generally formed during MS electrical ionization from carbonates, cyclic anhydrides and lactones (McLafferty and Turecek, 1993) indicating that the CO_2^+ is associated with -O-C-O- structure. Within the AMS, the CO_{2+} is also associated with decarboxylation of organic acids during heating followed by electrical ionization of the CO_2. We hypothesize that CO_2^+

15   formation from bicyclic peroxides is insignificant since CO_2 loss is not expected come from -C-O-O- structure during thermal decomposition. Therefore, it is the reaction products of bicyclic peroxides that lead to the formation of CO_2^+ and the difference in f_{44}. This indicates that the alkyl groups are more likely to contribute to SOA formation at the meta position than the ortho and para position. Bicyclic peroxides formed from the OH-addition reaction

20   pathway and their dissociation reaction products are both used to explain the substitute location impact on f_{44} and $f'_{43+57+71}$ relationship. However, the existence of longer alkyl substitutes diminishes the alkyl substitute location impact. SOA f_{44} and $f'_{43+57+71}$ in ethyltoluenes are all analogous to m-xylene. One substitute C_8 and C_9 aromatic hydrocarbons have similar f_{44} and $f'_{43+57+71}$ with slightly lower f_{44} and $f'_{43+57+71}$ compared to toluene (Li, et al.,

25   2016). Longer alkyl substitutes may not lower the average oxidation per mass as further oxidation of the longer chain alkyls may render other oxidized components not included in Fig. 2. Their lower total $f_{44}+f'_{43+57+71}$ (Fig. ~~S5~~S6) further supports the possibility of oxidation of the longer alkyl substitutes. It is also possible that oligomerization from highly oxidized carbonyls contribute more to the SOA formation from aromatics with long chain alkyl

substitute. Elemental ratio (Section 3.2.2) and oxidation state (Section 3.2.3) are further used to evaluate the impact of increasing alkyl group size on SOA formation.

3.2.2 H/C vs O/C

Elemental analysis (Aiken, et al., 2007, 2008) serves as a valuable tool to elucidate SOA

5   chemical composition and SOA formation mechanisms (Heald, et al., 2010; Chhabra, et al., 2011). Fig. ~~S7~~ S8 shows H/C and O/C evolution in SOA formed from the photooxidation of different aromatic hydrocarbons under low NO_x (marked and colored similarly to Fig. ~~S3~~S4). H/C and O/C ranges are comparable to previous chamber studies (Chhabra, et al., 2011 (*m*-xylene and toluene); Loza, et al., 2012 (*m*-xylene); Sato, et al., 2012 (benzene and 1, 3,

10   5-trimethylbenzene)). The SOA elemental ratio for C_8 and C_9 aromatic isomers are located near the alkyl number trend line found by Li, et al (2016) for methyl substituents, indicating a similarity between SOA from various alkyl substituted hydrocarbons. SOA formed is among the low volatility oxygenated organic aerosol (LV-OOA)and semi-volatile oxygenated organic aerosol (SV-OOA) regions (Ng, et al., 2011). The evolution trend agrees with Fig. ~~S3~~

15   S4 (Section 3.2.1), which means no significant H/C and O/C evolution is observed in the current study. Therefore, average H/C and O/C with standard deviation provided is used to explore the impact of molecular structure on SOA chemical composition. The current study concentrates on experimentally averaged H/C and O/C to explore the impact of molecular structure on SOA chemical composition.

20   Average H/C and O/C locations are marked with aromatic compound names in Fig. 3. All H/C and O/C are located around the predicted values for C_8 and C_9 SOA (dark solid circle) based on the elemental ratio of benzene SOA (Li, et al., 2016). This confirms the presence of a carbon dilution effect in all isomers. Ortho position aromatic hydrocarbons (*o*-xylene or *o*-ethyltoluene) lead to a more oxidized SOA (higher O/C and lower H/C) than that of meta

25   (*m*-xylene or *m*-ethyltoluene) and para (*p*-xylene or *p*-ethyltoluene) aromatics. SOA formed from 1, 2, 4-trimethylbenzene and 1, 2, 3-trimethylbenzene is more oxidized than that from 1, 3, 5-trimethylbenzene. It is noticed that 1, 2, 4-trimethylbenzene and 1, 2, 3-trimethylbenzene both contain an ortho position moiety on the aromatic ring. This indicates that the ortho

position aromatic hydrocarbon is readily oxidized and this ortho position impact on oxidation extends to triple substituted aromatic hydrocarbons. Substitute length also plays an important role in aromatic hydrocarbon oxidation. Overall, SOA from a one-substitute aromatic with more carbon in the substitute is located at a more oxidized area of the O/C vs. H/C chart

5   (lower right in Fig. 3.) than those multiple substitute aromatic isomers with the same total number of carbon as the single substituted aromatic. SOA from isopropylbenzene is located in a lower position of the chart and to the right of propylbenzene indicating that branch carbon structure on the alkyl substitute of aromatic hydrocarbons leads to a more oxidized SOA. Lines in Fig. S8 connect the O/C and H/C of resulting SOA to that of the aromatic precursor.

10   Most SOA components show a slight H/C increase and a dramatic O/C increase from the precursor, which is consistent with results observed for methyl substituted aromatics (Li, et al., 2016). However, H/C barely increases (1.33 to 1.34) from the propylbenzene precursor to its resulting SOA and there is even a decreasing trend from isopropylbenzene to its SOA. This indicates that a high H/C component loss reaction such as alkyl part dissociation during

15   photooxidation is an important reaction to SOA formation from longer carbon chain containing aromatic hydrocarbons. The carbon chain length of propylbenzene increases the possibility of alkyl fragmentation. The branching structure of isopropylbenzene facilitates fragmentation through the stability of tertiary alkyl radicals. Elemental ratio differences between xylenes and ethyltoluenes can be attributed to the alkyl dilution effect, similar to the

20   methyl dilution theory by Li, et al. (2016). Prediction of elemental ratios from toluene and xylenes are discussed later (Section 4) to further quantify the carbon length and branching effect on SOA formation from aromatic hydrocarbons.

3.2.3 OS_c

Oxidation state ($OS_c \approx 2O/C - H/C$) was introduced into aerosol phase component analysis by

25   Kroll et al. (2011). It is considered to be a more accurate metric for describing oxidation in atmospheric organic aerosol than H/C and O/C (Ng et al., 2009; Canagaratna, et al., 2015; Lambe, et al., 2015) and therefore well correlated with gas-particle partitioning (Aumont, et al., 2012;). Average OS_c of SOA formed from C_8 and C_9 aromatic isomers ranges from -0.54

to -0.17 and -0.82 to -0.22, respectively (Fig. 4), implying that the precursor molecular structure impacts the OS_c of the resulting SOA. An OS_c decrease with alkyl substitute length is observed in one-substitute aromatic hydrocarbons from toluene (toluene OS_c=-0.049; Li, et al. 2016) to propylbenzene. However, OS_c provides the average oxidation value per carbon

5   not considering whether these carbons start from an aromatic ring carbon or an alkyl carbon. Alkyl carbons are associated with more hydrogen than aromatic ring carbons, thus leading to a lower precursor OS_c and therefore lower SOA OS_c. Dilution conjecture in Section 4 will be used to further explore the carbon chain length effect on aromatic hydrocarbon oxidation by considering the precursor H:C ratio. Single substitute aromatic hydrocarbons generally show

10   higher OS_c than multiple substitute ones, consistent with the yield trend of Odum, et al (1997b). However, it is also found that ortho position moiety containing two or three substitute aromatic hydrocarbons have analogous or even higher OS_c to single substitute aromatic hydrocarbons (o-xylene -0.03±0.098 to ethylbenzene -0.173±0.033; 1,2,4-trimethylbenzene -0.425±0.072 and o-ethyltoluene -0.481±0.030 to propylbenzene

15   -0.421±0.111). This suggests that both substitute number and position are critical to aromatic hydrocarbon oxidation and therefore SOA formation. OS_c trends also support that the meta position suppresses oxidation while the ortho position promotes oxidation when the OS_c of xylenes (o-xylene>p-xylene>(insignificant) m-xylene), ethyltoluenes (o-ethyltoluene>p-ethyltoluene>(insignificant) m-ethyltoluene) and especially,

20   trimethylbenzenes (1, 2, 4-trimethylbenzene (ortho moiety containing)> (insignificant)1, 2, 3-trimethylbenzene (ortho moiety containing)>1, 3, 5-trimethylbenzene (meta moiety containing)) are compared separately. Further, SOA formed from isopropylbenzene shows the highest OS_c among all C_9 isomers, nearly equivalent to that of ethylbenzene. This demonstrates that the branching structure of the alkyl substitute can enhance further oxidation

25   of aromatic hydrocarbons.

3.3 Physical property

3.3.1 SOA Density

SOA density is a fundamental parameter in understanding aerosol morphology, dynamics, phase and oxidation (De Carol, et al., 2004; Katrib, et al., 2005; Dinar, et al., 2006; Cross, et al., 2007). SOA density ranges from 1.29-1.38 g/cm^3 from aromatic photooxidation under low NO_x conditions in this study (Fig. 5). The range is comparable to previous studies under similar conditions (Borrás and Tortajada-Genaro 2012; Ng, et al; 2007; Sato, et al., 2010). There is no significant difference in the density of SOA formed from C_8 and C_9 aromatic hydrocarbon isomers and molecular structure is not observed to be a critical parameter to determine SOA density. The standard deviation results from differences in initial conditions (e.g., initial HC/NO) that also determine the oxidation of aromatic hydrocarbons (Li, et al., 2015) and thus further affect density. SOA density is correlated with the O/C ratio and OS_c (0.551 and 0.540, Table 3), consistent with the observation of Pang, et al. (2006) that SOA density increases with increasing O/C ratio. The density prediction method developed by Kuwata, et al. (2011) based on O/C and H/C is evaluated as

$$\rho = \frac{12 + H/C + 16 \times O/C}{7 + 5 \times H/C + 4.15 \times O/C} \qquad \text{Eq-2}$$

The black lines (Fig. 5) are predicted (Eq-2) densities and show a good agreement between predicted and measured SOA densities (-6.01% ~ 7.62%). A comparatively large negative error is found in meta containing aromatic hydrocarbons including *m*-xylene, *m*-ethyltoluene and *1,3,5*-trimethylbenzene. It is noted that there should be more alkyl substitutes in SOA formed from meta position aromatics than other aromatics since meta position alkyl substitutes are more likely to participate into SOA products than other aromatics (Section 3.2.1 and Section 3.2.2). Previous work suggests that the increase of methyl groups could lead to a change in several key organic fragments (e.g., CO^+, CO_2^+ and H_2O^+) thereby altering the default fragment table for elemental ratio analysis. This agrees with the density underestimation in SOA formed from meta position aromatics and supports the preference of meta position alkyl substitute to SOA products.

3.3.2 SOA Volatility

SOA volatility is associated with reactions such as oxidation, fragmentation, oligomerization and mass loading (Kalberer, et al., 2004; Salo, et al., 2011; Tritscher, et al., 2011; Yu, et al., 2014). SOA volatility in this study is measured as VFR. Initial (<30 minutes after new particle formation) SOA VFRs are around 0.2 for all the aromatic precursors studied and increase up to 0.58 during photooxidation. This suggests that aromatic hydrocarbon oxidation undergoes an evolution from volatile compounds to semivolatile compounds. The VFR trends and ranges are comparable to previous studies (Kalberer et al., 2004; Qi et al., 2010a; Qi et al., 2010b; Nakao et al., 2012). Fig. 6 shows the VFR at the end of aromatic hydrocarbon photooxidation (VFR_{end}). A decreasing VFR_{end} trend is found as the number of substitutes increase and for meta position (e.g. m-xylene) or meta position containing (e.g. 1, 3, 5-trimethylbenzene) aromatic precursors. Correlations among VFR_{end} and chemical composition are observed in the aromatic hydrocarbons studied here (Table 3). This is consistent with recent findings that O:C ratio is correlated to aerosol volatility (Section 3.3.2) (Cappa, et al., 2012, Yu, et al., 2014), thereby affecting the gas-particle partitioning, which in turn relates to SOA yield. It is also observed that VFR_{end} is strongly correlated (-0.937) with reaction rate constant (k_{OH}). Higher k_{OH} is associated with faster reaction rates of initial aromatic precursors and is therefore expected to lead to further oxidation for a given reaction time. However, the inverse correlation between k_{OH} and VFR_{end} indicates that k_{OH} value represents more than just the kinetic aspects. k_{OH} increases with increasing number of substitutes on the aromatic ring. Additionally, aromatic hydrocarbons with meta position substitutes have higher k_{OH} than those with para and ortha (Table S1) position substitutes. This suggests that the precursor molecular structures for aromatics associated with k_{OH} values determine the extent of oxidation of the hydrocarbons and therefore impact SOA volatility more than simply the precursor oxidation rate.

4. Alkyl Dilution Conjecture on SOA formation from aromatic hydrocarbons

The dependence of SOA formation on molecular structure can be partially represented by the alkyl carbon number. Carbon dilution theory proposed by Li et al (2016) successfully explain that methyl group impacts remain similar in SOA elemental ratios as in the aromatic precursor. The chemical composition of SOA formation from alkyl substituted aromatics is predicted by simply adding the alkyl substitute into the chemical composition of SOA formed from pure aromatic ring precursor (benzene). Methyl dilution theory (Li, et al. 2016) is extended to alkyl substitute dilution conjecture in order to investigate the influence of longer alkyl substitutes compared with methyl group substitutes. A robust prediction of SOA H/C and O/C trends for longer (C2+) alkyl substituted aromatics based on the methyl substituted aromatics will suggest a similarity in the role of methyl and longer alkyl to SOA formation; an underestimation or overestimation will indicate different oxidation pathways for aromatics with differing alkyl substitute length. Fig. 7a and Fig. 7b shows the predicted elemental ratio and OS_c for SOA formed from longer alkyl substitutes (-C_nH_{2n+1}, n>1) based on methyl only substitute. The elemental ratio of SOA formed from single substitute aromatic hydrocarbons including ethylbenzene, propylbenzene and isopropylbenzene are predicted by toluene and those of ethyltoluenes are predicted by corresponding xylenes with similar alkyl substitute location. H/C and O/C are generally well predicted by alkyl dilution effect, expect for *o*-ethyltoluene and iso-propylbenzene. O/C (15%), H/C (1%) and OS_c (13%) of *o*-ethyltoluene are slightly overestimated by alkyl dilution effect. This indicates that *o*-ethyltoluene is less oxidized than *o*-xylene possibly due to the hindrance effect of the longer alkyl substitute.

OS_c is underestimated in SOA formed from single substitute aromatic hydrocarbons, especially for isopropylbenzene (-49%) and ethylbenzene (-25%). This implies that longer alkyl substitutes are more oxidized than the methyl group on toluene. A direct ·OH reaction with the alkyl part of the aromatic is more favored on longer alkyl chains since tertiary and secondary alkyl radicals are more stable than primary alkyl radicals (Forstner, et al., 1997). It

is also possible that oligomerization from highly oxidized carbonyl component might be more favored for long chain single alkyl substituted aromatics. The less significant OS_c underestimation from xylenes to ethyltoluenes (meta and para) is due to the presence of an "inert" methyl group which lowers the average OS_c. Fragmentation on alkyl substitute of

5   isopropylbenzene can lead to a higher OS_c (-0.22±0.04) than propylbenzene (-0.42$\pm$0.11), which possibly occurs while forming 2, 5-furandione or 3-H-furan-2-one due to the increased stability of the isopropyl radical compared to the n-propyl radical. It is also possible that longer carbon chain substitutes might have higher probability to form other cyclic or low vapor pressure products by additional reaction due to their increased length. The similarity in

10   f_{44} and $f'_{43+57+71}$ but discrepancy (insignificant) in elemental ratio among all single substitute C_8 and C_9 aromatics supports that additional reactions leading to further oxidization of alkyl substitutes can occur.

5. Atmospheric Implication

This study elucidates molecular structure impact on a major anthropogenic SOA source,

15   photooxidation of aromatic hydrocarbons, under atmospherically relevant NO_x conditions by analyzing SOA yield, chemical composition and physical properties. These observations, when taken together, indicate the roles of alkyl substitute number, location, carbon chain length and branching structure in aromatic hydrocarbon photooxidation. SOA yield of all C_8 and C_9 aromatic hydrocarbon isomers are comprehensively provided in this study with a focus

20   on the impact of molecular structure. It is demonstrated that aromatic hydrocarbon oxidation and SOA formation should not be simply explained by substitute number. The promoting of SOA formation by the ortho position is found along with confirmation of the suppression effect by the para position during oxidation of aromatic hydrocarbons. It is possible due to the alkyl substitute location impact on the further oxidation of five-membered bicyclic radicals.

25   Different carbonyl compounds can form as the ring opening products from the dissociation of five-membered bicyclic radical. It is assumed that oligomerization of these carbonyl compounds can contribute to SOA (Li, et al., 2016). Aromatic hydrocarbons with para position alkyl substitute tend to form more ketone like dicarbonyl compounds than other

aromatics. Ketone might contribute less to oligomerization formation compared with aldehyde as suggested in Li, et al (2016). Meta position alkyl substitutes on aromatic ring lead to a lower extent of aromatic hydrocarbon oxidation. It might be due to a higher percentage of carbonyl with alkyl substitute formed during the oxidation of meta containing aromatics (e.g. methylgloxal, 2-methyl-4-oxopent-2-enal), which contributes to oligomerization and thereby SOA formation. Evidence is provided to demonstrate aromatic oxidation increase with alkyl substitute chain length and branching structure. Further, carbon dilution theory developed by Li., et al (2016) is extended to this study. Carbon dilution theory not only serves as a tool to explain the difference in SOA components due to the difference in substitute alkyl carbon number but also acts as a standard to determine the oxidation mechanism based on alkyl substitute structure. Moreover, the five subcategories of aromatics and their two product modeling curve fitting parameters in this work at more realistic NO_x loadings provide a more precise prediction of SOA formation form aromatic hydrocarbons under atmospheric conditions. Previous studies found that the humidity insignificantly impacts SOA yield from aromatic hydrocarbons (Cocker, et al., 2001) or maintains the SOA yield relationship between isomers (Zhou, et al., 2001). Therefore, it is predicted that the observation found under dry conditions in this study, especially the molecular structure impact on SOA formation from different aromatic isomers could be extended to atmospherically relevant humidity conditions. However, recent studies observe that the hydration of carbonyls and epoxides could lead to further heterogeneous reaction and oligomerization (Jang, et al., 2002; Liggio, et al., 2005; Minerath and Elrod, et al., 2009; Lal, et al., 2012). It is possible that aerosol compositions and the hygroscopic properties could be altered after the heterogeneous reactions, especially under humid conditions. The impact of molecular structure impact on SOA formation under humidity condition needs to be further studied to extend the findings in current the work. This study improves the understanding of SOA formation from aromatic hydrocarbons and contributes to more accurate SOA prediction from aromatic precursors. Further study is warranted to reveal the detailed oxidation pathway of aromatic hydrocarbons with longer (carbon number >1) alkyl substitutes.

Acknowledgments

5 Reference

Aiken, A. C., DeCarlo, P. F., and Jimenez, J. L.: Elemental analysis of organic species with electron ionization high-resolution mass spectrometry, Anal. Chem., 79(21), 8350-8358, doi:10.1021/ac071150w, 2007.

Aiken, A. C., DeCarlo, P. F., Kroll, J. H., Worsnop, D. R., Huffman, J. A., Docherty, K. S.,
10 Ulbrich, I. M., Mohr, C., Kimmel, J. R., Sueper, D., Sun, Y., Zhang, Q., Trimborn, A., Northway, M., Ziemann, P. J., Canagaratna, M. R., Onasch, T. B., Alfarra, M. R., Prevot, A. S. H., Dommen, J., Duplissy, J., Metzger, A., Baltensperger, U., and Jimenez, J. H.: O/C and OM/OC ratios of primary, secondary, and ambient organic aerosols with high-resolution time-of-flight aerosol mass spectrometry, Environ. Sci. Technol., 42(12), 4478-4485,
15 doi:10.1021/es703009q, 2008.

Andino, J. M., Smith, J. N., Flagan, R. C., Goddard, W. A., and Seinfeld, J.H.: Mechanism of atmospheric photooxidation of aromatics: A theoretical study, J. Phys. Chem-US., 100(26), 10967-10980, doi: 10.1021/jp952935l, 1996.

Atkinson, R.: A structure‐activity relationship for the estimation of rate constants for the
20 gas‐phase reactions of OH radicals with organic compounds, Int. J. Chem. Kinet., 19(9), 799-828, doi: 10.1002/kin.550190903, 1987.

Atkinson, R., and Arey, J.: Atmospheric degradation of volatile organic compounds, Chem. Rev., 103(12), 4605-4638, doi:10.1021/cr0206420, 2003.

Aumont, B., Valorso, R., Mouchel-Vallon, C., Camredon, M., Lee-Taylor, J., and Madronich,
25 S.: Modeling SOA formation from the oxidation of intermediate volatility n-alkanes, Atmos. Chem. Phys., 12(16), 7577-7589, doi:10.5194/acp-12-7577-2012, 2012.

Bahreini, R., Ervens, B., Middlebrook, A., Warneke, C., De Gouw, J., DeCarlo, P., Jimenez, J., Brock, C., Neuman, J., Ryerson, T., Stark, H., Atlas, E., Brioude, J., Fried, A., Holloway, J. S., Peischl, J., Richter, D., Walega, J., Weibring, P., Wollny, A. G., and Fehsenfeld, F. C.:
30 Organic aerosol formation in urban and industrial plumes near Houston and Dallas, Texas, J. Geophys. Res.-Atmos., 114(D7), doi:10.1029/2008JD011493, 2009.

Borrás, E., and Tortajada-Genaro, L. A.: Secondary organic aerosol formation from the photo-oxidation of benzene, Atmos. Environ., 47, 154-163,doi:10.1016/j.atmosenv.2011.11.020, 2012.

Calvert, J. G., Atkinson, R., Becker, K. H., Kamens, R. M., Seinfeld, J. H., Wallington, T. J.,

5   and   Yarwood, G.: The mechanisms of atmospheric oxidation of aromatic hydrocarbons, Oxford University Press New York, 2002.

Canagaratna, M. R., Jayne, J. T., Jimenez, J. L., Allan, J. D., Alfarra, M. R., Zhang, Q., Onasch, T. B., Drewnick, F., Coe, H., Middlebrook, A., Delia, A., Williams, L. R., Trimborn, A. M., Northway, M. J., DeCarlo, P. F., Kolb, C. E., Davidovits, P., and Worsnop D. R.:

10 Chemical and microphysical characterization of ambient aerosols with the aerodyne aerosol mass spectrometer, Mass. Spectrom. Rev., 26(2), 185-222, doi:10.1002/mas.20115, 2007.

Canagaratna, M. R., Jimenez, J. L., Kroll, J. H., Chen, Q., Kessler, S. H., Massoli, P., Hildebrandt Ruiz, L., Fortner, E., Williams, L. R., Wilson, K. R., Surratt, J. D., Donahue, N. M., Jayne, J. T., and Worsnop, D. R.: Elemental ratio measurements of organic compounds

15 using aerosol mass spectrometry: characterization, improved calibration, and implications, Atmos. Chem. Phys., 15(1), 253-272, doi:10.5194/acp-15-253-2015, 2015.

Cappa, C. D., and Wilson, K. R.: Multi-generation gas-phase oxidation, equilibrium partitioning, and the formation and evolution of secondary organic aerosol, Atmos. Chem. Phys., 12(20), 9505-9528, doi:10.5194/acp-12-9505-2012, 2012.

20 Carter, W. P. L., Cocker III, D. R., Fitz, D. R., Malkina, I.L., Bumiller, K., Sauer, C.G., Pisano, J.T., Bufalino, C., Song, C.: A new environmental chamber for evaluation of gas-phase chemical mechanisms and secondary aerosol formation, Atmos. Environ., 39(40), 7768-7788, doi:10.1016/j.atmosenv.2005.08.040, 2005.

Carter, W. P. L., and Heo, G.: Development of Revised SAPRC Aromatics Mechanisms,

25 Atmos. Environ., 77, 404-414, doi:10.1016/j.atmosenv.2013.05.021, 2013.

Chhabra, P. S., Ng, N. L., Canagaratna, M. R., Corrigan, A. L., Russell, L. M., Worsnop, D. R., Flagan, R. C., and Seinfeld, J. H.: Elemental composition and oxidation of chamber organic aerosol, Atmos. Chem. Phys., 11(17), 8827-8845, doi:10.5194/acp-11-8827-2011,

30 2011.

Cocker III, D. R., Flagan, R. C., and Seinfeld, J. H.: State-of-the-art chamber facility for studying atmospheric aerosol chemistry, Environ. Sci. Technol., 35(12), 2594-2601, doi:10.1021/es0019169, 2001.

Correa, S. M., and Arbilla, G.: Aromatic hydrocarbons emissions in diesel and biodiesel exhaust. Atmos. Environ., 40(35), 6821-6826, doi: 10.1016/j.atmosenv.2006.05.068, 2006

Cross, E. S., Slowik, J. G., Davidovits, P., Allan, J. D., Worsnop, D. R., Jayne, J. T., Lewis, D. K., Canagaratna, M., and Onasch, T. B.: Laboratory and ambient particle density determinations using light scattering in conjunction with aerosol mass spectrometry, Aerosol Sci. Tech., 41(4), 343-359., doi:10.1080/02786820701199736, 2007.

Davidson, C. I., Phalen, R. F., and Solomon, P. A.: Airborne particulate matter and human health: A review, Aerosol Sci. Tech., 39(8), 737-749, doi: 10.1080/02786820500191348, 2005.

DeCarlo, P. F., Kimmel, J. R., Trimborn, A., Northway, M. J., Jayne, J. T., Aiken, A. C., Gonin, M., Fuhrer, K., Horvath, T., Docherty, K. S., Worsnop, D. R., and Jimenez, J. L.: Field-deployable, high-resolution, time-of-flight aerosol mass spectrometer. Anal. Chem., 78(24), 8281-8289, doi:10.1021/ac061249n, 2006.

DeCarlo, P. F., Slowik, J. G., Worsnop, D. R., Davidovits, P., and Jimenez, J. L.: Particle morphology and density characterization by combined mobility and aerodynamic diameter measurements. Part 1: Theory, Aerosol Sci. Tech., 38(12), 1185-1205, doi:10.1080/027868290903907, 2004.

Derwent, R. G., Jenkin, M. E., Utembe, S. R., Shallcross, D. E., Murrells, T. P., and Passant, N. R.: Secondary organic aerosol formation from a large number of reactive man-made organic compounds. Sci. Total. Environ., 408(16), 3374-3381, doi: 10.1016/j.scitotenv.2010.04.013, 2010.

Dinar, E., Mentel, T., and Rudich, Y.: The density of humic acids and humic like substances (HULIS) from fresh and aged wood burning and pollution aerosol particles, Atmos. Chem. Phys., 6(12), 5213-5224, doi:10.5194/acp-6-5213-2006, 2006.

Dockery, D. W., Pope, C. A., Xu, X., Spengler, J. D., Ware, J. H., Fay, M. E., Ferris Jr, B. G., and Speizer, F. E.: An association between air pollution and mortality in six US cities, New. Engl. J. Med., 329(24), 1753-1759, doi:10.1056/NEJM199312093292401, 1993.

Duplissy, J., DeCarlo, P. F., Dommen, J., Alfarra, M. R., Metzger, A., Barmpadimos, I., Prevot, A. S., Weingartner, E., Tritscher, T., and Gysel, M.: Relating hygroscopicity and composition of organic aerosol particulate matter, Atmos. Chem. Phys., 11(3), 1155-1165, doi:10.5194/acp-11-1155-2011, 2011.

Eddingsaas, N. C., Loza, C. L., Yee, L. D., Chan, M., Schilling, K. A., Chhabra, P. S., Seinfeld, J. H., and Wennberg, P. O.: α-pinene photooxidation under controlled chemical

conditions–Part 2: SOA yield and composition in low-and high-NO$_x$ environments, Atmos. Chem. Phys, 12(16), 7413-7427, doi:10.5194/acp-12-7413-2012, 2012.

Farina, S. C., Adams, P. J., and Pandis, S. N.: Modeling global secondary organic aerosol formation and processing with the volatility basis set: Implications for anthropogenic 5 secondary organic aerosol. J. Geophys. Res.-Atmos., 115(D9), doi: 10.1029/2009JD013046, 2010.

Fisseha, R., Dommen, J., Sax, M., Paulsen, D., Kalberer, M., Maurer, R., Höfler, F., Weingartner, E., and Baltensperger, U.: Identification of organic acids in secondary organic aerosol and the corresponding gas phase from chamber experiments, Anal. Chem., 76(22), 10 6535-6540, doi: 10.1021/ac048975f, 2004.

Forstner, H. J. L., Flagan, R. C., and Seinfeld, J. H.: Secondary organic aerosol from the photooxidation of aromatic hydrocarbons: Molecular composition, Environ. Sci. Technol., 31(5), 1345-1358, doi:10.1021/es9605376, 1997.

Hallquist, M., Wenger, J. C., Baltensperger, U., Rudich, Y., Simpson, D., Claeys, M., 15 Dommen, J., Donahue, N. M., George, C., Goldstein, A. H., Hamilton, J. F., Herrmann, H., Hoffmann, T., Iinuma, Y., Jang, M., Jenkin, M. E., Jimenez, J. L., Kiendler-Scharr, A., Maenhaut, W., McFiggans, G., Mentel, Th. F., Monod, A., Prévôt, A. S. H., Seinfeld, J. H., Surratt, J. D., Szmigielski, R., and Wildt, J.: The formation, properties and impact of secondary organic aerosol: current and emerging issues, Atmos. Chem. Phys., 9(14), 20 5155-5236, doi:10.5194/acp-9-5155-2009, 2009.

Hamilton, J. F., Webb, P. J., Lewis, A. C., and Reviejo, M. M.: Quantifying small molecules in secondary organic aerosol formed during the photo-oxidation of toluene with hydroxyl radicals, Atmos. Environ., 39(38), 7263-7275, doi:10.1016/j.atmosenv.2005.09.006, 2005.

Heald, C. L., Goldstein, A. H., Allan, J. D., Aiken, A. C., Apel, E., Atlas, E. L., Baker, A. K., 25 Bates, T. S., Beyersdorf, A. J., Blake, D. R., A., Campos, T., Coe, H., Crounse, J. D., DeCarlo, P. F., de Gouw, J. A., Dunlea, E. J., Flocke, F. M., Fried, Goldan, P., Griffin R. J., Herndon, S. C., Holloway, J. S., Holzinger, R., Jimenez J. L., Junkermann, W., Kuster, W. C., Lewis, A. C., Meinardi, S., Millet, D. B., Onasch, T., Polidori, A., Quinn, P. K., Riemer, D. D., Roberts, J. M., Salcedo, D., Sive, B., Swanson, A. L., Talbot, R., Warneke, C., Weber, R. 30 J., Weibring, P., Wennberg, P. O., Worsnop, D. R., Wittig, A. E., Zhang, R., Zheng, J., and Zheng, W.: Total observed organic carbon (TOOC) in the atmosphere: a synthesis of North American observations, Atmos. Chem. Phys., 8(7), 2007-2025.doi: 10.5194/acp-8-2007-2008, 2008.

Heald, C. L., Kroll, J. H., Jimenez, J. L., Docherty, K. S., DeCarlo, P. F., Aiken, A. C., Chen, 35 Q., Martin, S. T., Farmer, D. K., and Artaxo, P.: A simplified description of the evolution of

organic aerosol composition in the atmosphere, Geophys. Res. Lett, 37(8), doi:10.1029/2010GL042737, 2010.

Henze, D. K., Seinfeld, J. H., Ng, N. L., Kroll, J. H., Fu, T-M., Jacob, D. J., and Heald, C. L.: Global modeling of secondary organic aerosol formation from aromatic hydrocarbons: high-vs. low-yield pathways, Atmos. Chem. Phys., 8(9), 2405-2421, doi:10.5194/acp-8-2405-2008, 2008.

Hu, L., Millet, D. B., Baasandorj, M., Griffis, T. J., Travis, K. R., Tessum, C. W., Marshall, J. D., Reinhart, W. F., Mikoviny, T., Müller, M., Wisthaler, A., Graus, M., Warneke, C., and de Gouw, J.:Emissions of C_6–C_8 aromatic compounds in the United States: Constraints from tall tower and aircraft measurements, J. Geophys. Res.-Atmos., 120(2), 826-842, doi:10.1002/2014JD022627, 2015.

Huang, M., Wang, Z., Hao, L., and Zhang, W.: Theoretical investigation on the mechanism and kinetics of OH radical with ethylbenzene: Int. J. Quantum. Chem., 111(12), 3125-3134, doi: 10.1002/qua.22751, 2011

Huang, M., Zhang, W., Hao, L., Wang, Z., Zhao, W., Gu, X., Guo, X., Liu, X., Long, B., and Fang, L.: Laser desorption/ionization mass spectrometric study of secondary organic aerosol formed from the photooxidation of aromatics, J. Atmos. Chem., 58(3), 237-252, doi: 10.1007/s10874-007-9090-x, 2007.

IPCC.: Intergovernmental Panel on Climate Change: Climate Change 2007: The Physical Science Basis, Cambridge University Press, UK, 6, 07, 2007.

Izumi, K., and Fukuyama, T. : Photochemical aerosol formation from aromatic hydrocarbons in the presence of NO_x, Atmos. Environ. A-Gen., 24(6), 1433-1441, doi: 10.1016/0960-1686(90)90052-O, 1990.

Jang, M., Czoschke, N. M., Lee, S., and Kamens, R. M.: Heterogeneous atmospheric aerosol production by acid-catalyzed particle-phase reactions, Science, 298(5594), 814-817, doi:10.1126/science.1075798, 2002.

Jimenez, J. L., Canagaratna, M. R., Donahue, N. M., Prevot, A. S. H., Zhang, Q., Kroll, J. H., DeCarlo, P. F., Allan, J. D., Coe, H., Ng, N. L., Aiken, A. C., Docherty, K. S., Ulbrich, I. M., Grieshop, A. P., Robinson, A. L., Duplissy, J., Smith, J. D., Wilson, K. R., Lanz, V. A., Hueglin, C., Sun, Y. L., Tian, J., Laaksonen, A., Raatikainen, T., Rautiainen, J., Vaattovaara, P., Ehn, M., Kulmala, M., Tomlinson, J. M., Collins, D. R., Cubison, M. J., Dunlea1, E., J., Huffman, J. A., Onasch, T. B., Alfarra, M. R., Williams, P. I., Bower, K., Kondo, Y., Schneider, J., Drewnick, F., Borrmann, S., Weimer, S.,, Demerjian, K., Salcedo, D., Cottrell, L., Griffin, R., Takami, A., Miyoshi, T., Hatakeyama, S., Shimono, A., Sun, J. Y., Zhang, Y.

M., Dzepina, K., Kimmel, J. R., Sueper, D., J. Jayne, T.,   Herndon, S. C., Trimborn, A. M., Williams, L. R., Wood, E. C., Middlebrook, A. M., Kolb C. E., Baltensperger, U. and Worsnop D. R.: Evolution of organic aerosols in the atmosphere, Science, 326(5959), 1525-1529, doi:10.1126/science.1180353, 2009.

5   Kaiser, E. W., Siegl, W. O., Cotton, D. F., and Anderson, R.W.: Effect of fuel structure on emissions from a spark-ignited engine. 2. Naphthene and aromatic fuels, Environ. Sci. Technol., 26(8), 1581-1586, doi: 10.1021/es00032a014, 1992.

Kalberer, M., Paulsen, D., Sax, M., Steinbacher, M., Dommen, J., Prevot, A. S. H., Fisseha, R., Weingartner, E., Frankevich, V., and Zenobi, R.: Identification of polymers as major
10   components of atmospheric organic aerosols, Science, 303(5664), 1659-1662, doi:10.1126/science.1092185, 2004.

Kanakidou, M., Seinfeld, J. H., Pandis, S. N., Barnes, I., Dentener, F. J, Facchini, M. C., Van Dingenen, R., Ervens, B., Nenes, A., Nielsen, C. J., Swietlicki, E., Putaud, J. P., Balkanski, Y., Fuzzi, S., Horth, J., Moortgat, G. K., Winterhalter, R., Myhre, C. E. L., Tsigaridis, K.,
15   Vignati, E., Stephanou, E. G., and Wilson, J.: Organic aerosol and global climate modelling: a review, Atmos. Chem. Phys., 5(4), 1053-1123, doi:10.5194/acp-5-1053-2005, 2005.

Kansal, A.: Sources and reactivity of NMHCs and VOCs in the atmosphere: a review, J. Hazard. Mater, 166(1), 17-26, doi: 10.1016/j.jhazmat.2008.11.048., 2009.

Katrib, Y., Martin, S. T., Rudich, Y., Davidovits, P., Jayne, J. T., and Worsnop, D. R.:
20   Density changes of aerosol particles as a result of chemical reaction, Atmos. Chem. Phys., 5(1), 275-291, doi:10.5194/acp-5-275-2005, 2005.

Krewski, D., Burnett, R., Goldberg, M., Hoover, B.K., Siemiatycki, J., Jerrett, M., Abrahamowicz, M., and White, W. : Overview of the reanalysis of the Harvard six cities study and American Cancer Society study of particulate air pollution and mortality, Toxicol.
25   Env. Heal. A., 66(16-19), 1507-1552, doi: 10.1080/15287390306424, 2003.

Kuwata, M., Zorn, S. R., and Martin, S. T.: Using elemental ratios to predict the density of organic material composed of carbon, hydrogen, and oxygen, Environ. Sci. Technol., 46(2), 787-794, doi:10.1021/es202525q, 2011.

Lal, V., Khalizov, A. F., Lin, Y., Galvan, M. D., Connell, B. T., and Zhang, R.:
30   Heterogeneous reactions of epoxides in acidic media. J. Phys. Chem. A., 116(24), 6078-6090, doi: 10.1021/jp2112704. 2012.

Lambe, A. T., Onasch, T. B., Croasdale, D. R., Wright, J. P., Martin, A. T., Franklin, J. P., Massoli, P., Kroll, J. H., Canagaratna, M. R., Brune, W. H., Worsnop D. R., and Davidovits P.: Transitions from functionalization to fragmentation reactions of laboratory secondary

organic aerosol (SOA) generated from the OH oxidation of alkane precursors, Environ. Sci. Technol., 46(10), 5430-5437, doi: 10.1021/es300274t, 2012.

Lambe, A. T., Chhabra, P. S., Onasch, T. B., Brune, W. H., Hunter, J. F., Kroll, J. H., Cummings, M. J., Brogan, J. F., Parmar, Y., Worsnop, D. R., Kolb, C. E., and Davidovits, P.:

5   Effect of oxidant concentration, exposure time, and seed particles on secondary organic aerosol chemical composition and yield, Atmos. Chem. Phys., 15(6), 3063-3075, doi:10.5194/acp-15-3063-2015, 2015.Li, L., Tang, P., Nakao, S., Chen, C.-L., and Cocker III, D. R.: Role of methyl group number on SOA formation from aromatic hydrocarbons photooxidation under low-NO$_x$ conditions, Atmos. Chem. Phys., 16, 2255–2272,

10   doi:10.5194/acp-16-2255-2016, 2016

Li, L.; Tang, P., Cocker III, D. R.: Instantaneous nitric oxide effect on secondary organic aerosol formation from *m*-xylene photooxidation. Atmos. Environ., 119, 144-155, doi:10.1016/j.atmosenv.2015.08.010, 2015.

Liggio, J., Li, S.-M., and McLaren R.: Heterogeneous reactions of glyoxal on particulate

15   matter: Identification of acetals and sulfate esters, Environ. Sci. Technol. 39(6): 1532-1541, dio: 10.1021/es048375y, 2005.

Lim, Y. B., and Ziemann, P. J.: Effects of molecular structure on aerosol yields from OH radical-initiated reactions of linear, branched, and cyclic alkanes in the presence of NO$_x$, Environ. Sci. Technol., 43(7), 2328-2334, doi:10.1021/es803389s, 2009.

20   Lough, G. C., Schauer, J. J., Lonneman, W. A., and Allen, M. K.: Summer and winter nonmethane hydrocarbon emissions from on-road motor vehicles in the Midwestern United States, J. Air. Waste. Manage., 55(5), 629-646, doi: 10.1080/10473289.2005.10464649, 2005

Loza, C. L., Chhabra, P. S., Yee, L. D., Craven, J. S., Flagan, R. C. and Seinfeld, J. H.: Chemical aging of *m*-xylene secondary organic aerosol: laboratory chamber study, Atmos.

25   Chem. Phys., 12(1), 151-167, doi:10.5194/acp-12-151-2012, 2012.

Loza, C. L., Craven, J. D., Yee, L. D., Coggon, M. M., Schwantes, R. H., Shiraiwa, M., Zhang, X., Schilling, K. A, Ng, N. L., Canagaratna, M. R., Ziemann, P. J., Flagan, R. C., and Seinfeld, J. H.: Secondary organic aerosol yields of 12-carbon alkanes. Atmos. Chem. Phys., 14(3), 1423-1439, doi: 10.5194/acp-14-1423-2014, 2014.

30   Malloy, Q. G., Nakao, S., Qi, L., Austin, R., Stothers, C., Hagino, H., and Cocker III, D. R.: Real-Time Aerosol Density Determination Utilizing a Modified Scanning Mobility Particle Sizer—Aerosol Particle Mass Analyzer System, Aerosol. Sci. Tech., 43(7), 673-678.doi:10.1080/02786820902832960, 2009.

Matsui, H., Koike, M., Takegawa, N., Kondo, Y., Griffin, R., Miyazaki, Y., Yokouchi, Y., and Ohara, T.: Secondary organic aerosol formation in urban air: Temporal variations and possible contributions from unidentified hydrocarbons, J. Geophys. Res.-Atmos, 114(D4), D04201, doi: 10.1029/2008JD010164, 2009.

5   McLafferty, F. W., and Turecek, F.: Interpretation of mass spectra. University Science Books, , Mill Valley, California, 1993.

Millet, D. B., Donahue, N. M., Pandis, S. N., Polidori, A., Stanier, C. O., Turpin, B. J., and Goldstein, A. H.: Atmospheric volatile organic compound measurements during the Pittsburgh Air Quality Study: Results, interpretation, and quantification of primary and

10   secondary contributions, J. Geophys. Res.-Atmos, 110(D7), D07S07, doi:10.1029/2004JD004601, 2005

Minerath, E. C. and Elrod, M. J.: Assessing the potential for diol and hydroxy sulfate ester formation from the reaction of epoxides in tropospheric aerosols. Environ. Sci. Technol., 43(5), 1386–1392, doi: 10.1021/es8029076, 2009

15   Miracolo, M. A., Drozd, G. T., Jathar, S. H., Presto, A. A., Lipsky, E. M., Corporan, E., and Robinson, A.L.: Fuel composition and secondary organic aerosol formation: Gas-turbine exhaust and alternative aviation fuels. Environ. Sci. Technol., 46(15), 8493-8501, doi: 10.1021/es300350c, 2012.Monod, A., Sive, B. C., Avino, P., Chen, T., Blake, D. R., and Rowland, F. S.: Monoaromatic compounds in ambient air of various cities: a focus on

20   correlations between the xylenes and ethylbenzene, Atmos. Environ., 35(1), 135-149, doi: 10.1016/S1352-2310(00)00274-0, 2001.

Na, K., Moon, K.-C., and Kim, Y. P.: Source contribution to aromatic VOC concentration and ozone formation potential in the atmosphere of Seoul. Atmos. Environ., 39(30), 5517-5524, doi: 10.1016/j.atmosenv.2005.06.005, 2005.

25   Nakao, S., Clark, C., Tang, P., Sato, K., and Cocker III, D.: Secondary organic aerosol formation from phenolic compounds in the absence of NO_x, Atmos. Chem. Phys., 11, 10649-10660, doi:10.5194/acp-11-10649-2011, 2011.

Nakao, S., Liu, Y., Tang, P., Chen, C.-L., Zhang, J., and Cocker III, D. R.: Chamber studies of SOA formation from aromatic hydrocarbons: observation of limited glyoxal uptake,

30   Atmos. Chem. Phys., 12(9), 3927-3937, doi:10.5194/acp-12-3927-2012, 2012.

Ng, N. L., Canagaratna, M. R., Jimenez, J. L., Chhabra, P. S., Seinfeld, J. H., and Worsnop, D. R.: Changes in organic aerosol composition with aging inferred from aerosol mass spectra, Atmos. Chem. Phys., 11(13), 6465-6474, doi:10.5194/acp-11-6465-2011, 2011.

Ng, N. L., Canagaratna, M. R., Zhang, Q., Jimenez, J. L., Tian, J., Ulbrich, I. M., Kroll, J. H., Docherty, K. S., Chhabra, P. S., Bahreini, R., Murphy, S. M., Seinfeld, J. H., Hildebrandt, L., Donahue, N. M., DeCarlo, P. F., Lanz, V. A., Prévôt, A. S. H., Dinar E., Rudich Y., and Worsnop D. R.: Organic aerosol components observed in Northern Hemispheric datasets from

5   Aerosol Mass Spectrometry, Atmos. Chem. Phys., 10(10), 4625-4641, doi:10.5194/acp-10-4625-2010, 2010.

Ng, N. L., Kroll, J. H., Chan, A. W. H., Chhabra, P. S., Flagan, R. C., and Seinfeld, J. H.: Secondary organic aerosol formation from *m*-xylene, toluene, and benzene, Atmos. Chem. Phys., 7(14), 3909-3922, doi: 10.5194/acp-7-3909-2007, 2007.

10   Odum, J. R., Hoffmann, T., Bowman, F., Collins, D., Flagan, R. C., and Seinfeld, J. H.: Gas/particle partitioning and secondary organic aerosol yields, Environ. Sci. Technol., 30(8), 2580-2585, doi:10.1021/es950943+, 1996.

Odum, J. R., Jungkamp, T., Griffin, R., Flagan, R. C., and Seinfeld, J. H.: The atmospheric aerosol-forming potential of whole gasoline vapor, Science, 276(5309), 96-99,

15   doi:10.1126/science.276.5309.96, 1997a.

Odum, J. R., Jungkamp, T., Griffin, R. J., Forstner, H., Flagan, R. C., and Seinfeld, J.H.: Aromatics, reformulated gasoline, and atmospheric organic aerosol formation, Environ. Sci. Technol., 31(7), 1890-1897, doi:10.1021/es960535l, 1997b.

Pöschl, U.: Atmospheric aerosols: Composition, transformation, climate and health effects,

20   Angew. Chem. Int. Edit., 44(46), 7520-7540, 10.1002/anie.200501122, 2005.

Pang, Y., Turpin, B., and Gundel, L.: On the importance of organic oxygen for understanding organic aerosol particles, Aerosol. Sci. Tech., 40(2), 128-133, doi:10.1080/02786820500423790, 2006.

Pfaffenberger, L., Barmet, P., Slowik, J. G., Praplan, A. P., Dommen, J., Prévôt, A. S. H., and

25   Baltensperger, U. : The link between organic aerosol mass loading and degree of oxygenation: an α-pinene photooxidation study, Atmos. Chem. Phys., 13(13), 6493-6506, doi:10.5194/acp-13-6493-2013, 2013.

Qi, L., Nakao, S., Malloy, Q., Warren, B., and Cocker III, D. R.: Can secondary organic aerosol formed in an atmospheric simulation chamber continuously age? Atmos. Environ.,

30   44(25), 2990-2996, doi:10.1016/j.atmosenv.2010.05.020, 2010a.

Qi, L., Nakao, S., Tang, P., and Cocker III, D. R.: Temperature effect on physical and chemical properties of secondary organic aerosol from *m*-xylene photooxidation, Atmos. Chem. Phys., 10(8), 3847-3854, doi:10.5194/acp-10-3847-2010, 2010b.

Rader, D. J. and McMurry, P. H.: Application of the tandem differential mobility analyzer to studies of droplet growth or evaporation, J. Aerosol. Sci., 17(5), 771-787, doi:10.1016/0021-8502(86)90031-5, 1986.

Rubin, J. I., Kean, A. J., Harley, R. A., Millet, D. B., and Goldstein, A. H.: Temperature dependence of volatile organic compound evaporative emissions from motor vehicles. J. Geophys. Res.-Atmos, 111(D3), 10.1029/2005JD006458, 2006.

Salo, K., Hallquist, M., Jonsson, Å.M., Saathoff, H., Naumann, K.-H., Spindler, C., Tillmann, R., Fuchs, H., Bohn, B., Rubach, F., Mentel, T. F., Müller, L., Reinnig, M., Hoffmann, T., and Donahue, N. M.: Volatility of secondary organic aerosol during OH radical induced ageing, Atmos. Chem. Phys., 11(21), 11055-11067, doi:10.5194/acp-11-11055-2011, 2011.

Sato, K., Hatakeyama, S., and Imamura, T.: Secondary organic aerosol formation during the photooxidation of toluene: NO_x dependence of chemical composition, J. Phys. Chem. A., 111(39), 9796-9808, doi:10.1021/jp071419f, 2007.

Sato, K., Takami, A., Isozaki, T., Hikida, T., Shimono, A., and Imamura, T.: 2010. Mass spectrometric study of secondary organic aerosol formed from the photo-oxidation of aromatic hydrocarbons, Atmos. Environ., 44(8), 1080-1087, doi:10.1016/j.atmosenv.2009.12.013, 2010.

Sato, K., Takami, A., Kato, Y., Seta, T., Fujitani, Y., Hikida, T., Shimono, A., and Imamura, T. 2012. AMS and LC/MS analyses of SOA from the photooxidation of benzene and 1, 3, 5-trimethylbenzene in the presence of NO_x: effects of chemical structure on SOA aging, Atmos. Chem. Phys, 12, 4667-4682, doi:10.5194/acp-12-4667-2012, 2012.

Seinfeld, J. and Pandis, S.: Atmospheric chemistry and physics: from air pollution to climate change. John Wiley & Sons Publications, Hoboken, New Jersey, US, 2006.

Shilling, J. E., Chen, Q., King, S. M., Rosenoern, T., Kroll, J. H., Worsnop, D. R., DeCarlo, P. F., Aiken, A. C., Sueper, D., Jimenez, J. L., and Martin, S. T.: Loading-dependent elemental composition of α-pinene SOA particles, Atmos. Chem. Phys., 9(3), 771-782, doi:10.5194/acp-9-771-2009, 2009.

Singh, H. B., Salas, L. J., Cantrell, B. K., and Redmond, R. M.: Distribution of aromatic hydrocarbons in the ambient air, Atmos. Environ., (1967), 19(11), 1911-1919, doi:10.1016/0004-6981(85)90017-4, 1985.

Song, C., Na, K., and Cocker III, D. R.: Impact of the hydrocarbon to NO_x ratio on secondary organic aerosol formation, Environ. Sci. Technol., 39(9), 3143-3149, doi:10.1021/es0493244, 2005.

Song, C., Na, K., Warren, B., Malloy, Q., Cocker III, D. R.: Secondary organic aerosol formation from the photooxidation of *p*-and *o*-xylene. Environ. Sci. Technol., 41(21), 7403-7408, doi: 10.1021/es0621041, 2007.

Tkacik, D. S., Presto, A. A., Donahue, N. M., and Robinson, A. L.: Secondary organic aerosol formation from intermediate-volatility organic compounds: cyclic, linear, and branched alkanes, Environ. Sci. Technol., 46(16), 8773-8781, doi:10.1021/es301112c, 2012.

Tritscher, T., Dommen, J., DeCarlo, P. F., Gysel, M., Barmet, P. B., Praplan, A. P., Weingartner, E., Prévôt, A. S. H., Riipinen, I., Donahue, N. M., and Baltensperger, U.: Volatility and hygroscopicity of aging secondary organic aerosol in a smog chamber, Atmos. Chem. Phys., 11(22), 11477-11496, doi:10.5194/acp-11-11477-2011, 2011.

Yee, L. D., Kautzman, K. E., Loza, C. L., Schilling, K. A., Coggon, M. M., Chhabra, P. S., Chan, M. N., Chan, A. W. H, Hersey, S., Crounse, J. Wennberg, P. O., Flagan, R. C., and Seinfeld, J. H.: Secondary organic aerosol formation from biomass burning intermediates: phenol and methoxyphenols. Atmos. Chem. Phys., 13(16), 8019-8043, doi: 10.5194/acp-13-8019-2013, 2013.

Yu, L., Smith, J., Laskin, A., Anastasio, C., Laskin, J., and Zhang, Q.: Chemical characterization of SOA formed from aqueous-phase reactions of phenols with the triplet excited state of carbonyl and hydroxyl radical, Atmos. Chem. Phys., 14(24), 13801-13816, doi:10.5194/acp-14-13801-2014, 2014.

Zhang, Q., Alfarra, M. R., Worsnop, D. R., Allan, J. D., Coe, H., Canagaratna, M. R., and Jimenez, J. L.: Deconvolution and quantification of hydrocarbon-like and oxygenated organic aerosols based on aerosol mass spectrometry, Environ. Sci. Technol., 39(13), 4938-4952, doi:10.1021/es048568l, 2005.

Zhang, Y., Wang, X., Barletta, B., Simpson, I.J., Blake, D.R., Fu, X., Zhang, Z., He, Q., Liu, T., Zhao, X., and Ding, X.: Source attributions of hazardous aromatic hydrocarbons in urban, suburban and rural areas in the Pearl River Delta (PRD) region. J. Hazard. Mater., 250, 403-411, doi: 10.1016/j.jhazmat.2013.02.023, 2013.

Ziemann, P.: Effects of molecular structure on the chemistry of aerosol formation from the OH-radical-initiated oxidation of alkanes and alkenes, International Reviews in Physical Chemistry, 30(2), 161-195, doi:10.1080/0144235X.2010.550728, 2011.

Ziemann, P.J., and Atkinson, R.: Kinetics, products, and mechanisms of secondary organic aerosol formation. Chem. Soc. Rev., 41(19), 6582-6605, doi: 10.1039/c2cs35122f, 2012

Table 1. Experiment conditions

Precursor	ID	HC/NO ppbC:ppb	NO ppb	HC ppb	ΔHC µg·m^{-3}	M$_o$^{a} µg·m^{-3}	Yield
Ethylbenzene	1142A	17.0	47.4	101	331	22.0	0.066
	1142B	12.0	66.6	99.9	341	4.40	0.013
	1146A	35.6	22.2	99.0	257	36.0	0.140
	1146B	23.0	34.8	100	331	23.6	0.071
	1147B	74.9	36.5	342	626	88.1	0.141
	2084A	81.1	23.9	242	374	54.0	0.145
	2084B	93.8	20.3	238	266	44.3	0.167
Propylbenzene	1245A	41.0	22.1	101	231	11.8	0.051
	1246A	26.8	68.5	204	421	22.9	0.054
Isopropylbenzene	1247A	40.3	22.4	100	301	33.2	0.110
	1247B	18.6	48.1	99.3	300	16.6	0.055
	1253A	31.9	56.4	200.	538	53.1	0.099
	1253B*	17.6	100	196	526	16.5	0.031
o-Xylene	1315A	13.2	49.8	82.2	324	26.3	0.081
	1315B	28.8	22.2	80.0	27	25.4	0.091
	1320A	12.8	50.0	80.0	335	18.4	0.055
	1321A	31.0	20.5	79.2	263	16.2	0.061
	1321B	61.3	10.4	80.0	226	9.80	0.044
p-Xylene	1308A	15.5	55.6	78.4	279	6.80	0.024
	1308B	171	22.9	78.8	274	11.3	0.041
m-Ethyltoluene	1151A	17.9	62.5	84.8	409	8.30	0.020
	1151B	31.0	32.3	86.4	415	28.7	0.069
	1199A	8.8	45.4	100.2	447	72.0	0.161
	1222B	41.7	69.4	100.0	484	70.9	0.146
	1226B	11.3	137.6	201.1	895	138	0.154
	1232A	27.5	122.0	200.0	901	150	0.167
	1232B	33.1	67.5	194.8	751	117	0.155
	1421A	41.0	22.1	97.9	409	46.2	0.112
	1421B	18.0	44.9	98.7	477	54.6	0.114
o-Ethyltoluene	1179A	16.3	52.9	91.7	399	86.5	0.216
	1179B	15.8	52.9	93.0	415	75.3	0.181
	1202A	18.5	60.3	99.7	422	69.9	0.166
	1215A	29.2	107.9	180.3	637	151	0.237
	1413A	12.2	21.3	100.4	371	64.5	0.174
	1413B	24.1	45.8	98.4	455	64.4	0.141
p-Ethyltoluene	1194A	19.9	90.7	196	741	90.4	0.122
	1194B	13.0	88.4	200	761	73.0	0.096
	1197A	13.1	56.4	192	653	66.4	0.102
	1197B	14.8	98.5	192	710	58.4	0.082
	1214B	26.0	53.4	102	418	29.1	0.069
	1601A	39.9	31.2	109	452	17.6	0.039
1, 2, 3-Trimethylbenzene	1158A	19.8	10.3	79.9	296	22.2	0.075
	1158B	15.6	22.4	79.9	379	32.3	0.085
	1162A	15.8	33.4	80.1	391	46.5	0.119
	1162B	14.9	40.0	80.4	399	46.6	0.117
1, 3, 5-Trimethylbenzene	1153A	65.2	11.0	79.5	309	12.4	0.040
	1153B	35.3	20.4	80.0	381	19.6	0.051

1156A	22.3	32.3	80.2	379	24.8	0.065
1156B	15.5	46.1	79.6	390	19.0	0.049
1329B	11.1	64.8	80.0	296	3.00	0.007

Note: a) M_o is a wall loss and density corrected particle mass concentration; * Not used in curve fitting

Table 2. Two product yield curve fitting parameters for one, two (ortha, meta and para) and three alkyl substitutes

Yield Curve	α_1	$K_{om,1}$ $(m^3 \cdot \mu g^{-1})$	α_2	$K_{om,2}$ $(m^3 \cdot \mu g^{-1})$	MSRE[a]
One Substitutes	0.144	0.039	0.137	0.005	5.38
Two Substitutes-ortho	0.158	0.249	0.024	0.005	2.03
Two Substitutes-meta	0.156	0.040	0.080	0.005	2.51
Two Substitutes-para	0.154	0.025	0.036	0.005	1.21
Three Substitutes	0.180	0.025	0.052	0.005	0.84

Note: a) Mean squared error (MSRE)= [(Fitted Yield - Measured Yield)/ Measured Yield]^2/(Number of Data Points)

5   Table 3. Correlation among SOA density, volatility (VFR) and SOA chemical composition

	f_{44}	f_{57}	f_{71}	O/C	H/C	OS_c	k_{OH}
Density	0.324	-0.056	-0.38	0.551	-0.301	0.540	-0.249
p-value[b]	0.304	0.862	0.223	0.063	0.341	0.070	0.435
VFR_{end}[a]	0.537	0.56	0.399	0.471	-0.586	0.593	-0.937
p-value[b]	0.089	0.073	0.224	0.144	0.058	0.055	0.000

Note: a) VFR_{end} volume fraction remaining at the end of photooxidation; b) p-Values range from 0 to 1, 0-reject null hypothesis and 1 accept null hypothesis. Alpha (α) level used is 0.05. If the p-value of a test statistic is less than alpha, the null hypothesis is rejected
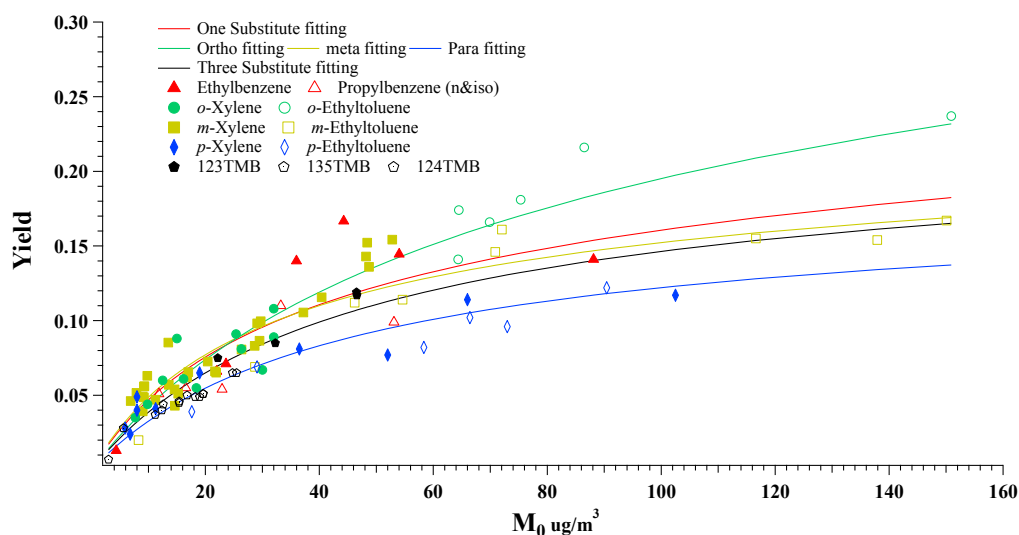
10

Note: Song, et al, 2005; Song, et al, 2007; Li, et al., 2016 data are also included; 123TMB- 1, 2, 3-Trimethylbenzene; 135TMB- 1, 3, 5-Trimethylbenzene; 124TMB- 1, 2, 4-Trimethylbenzene.

Fig.1. Aromatic SOA yields as a function of M_o
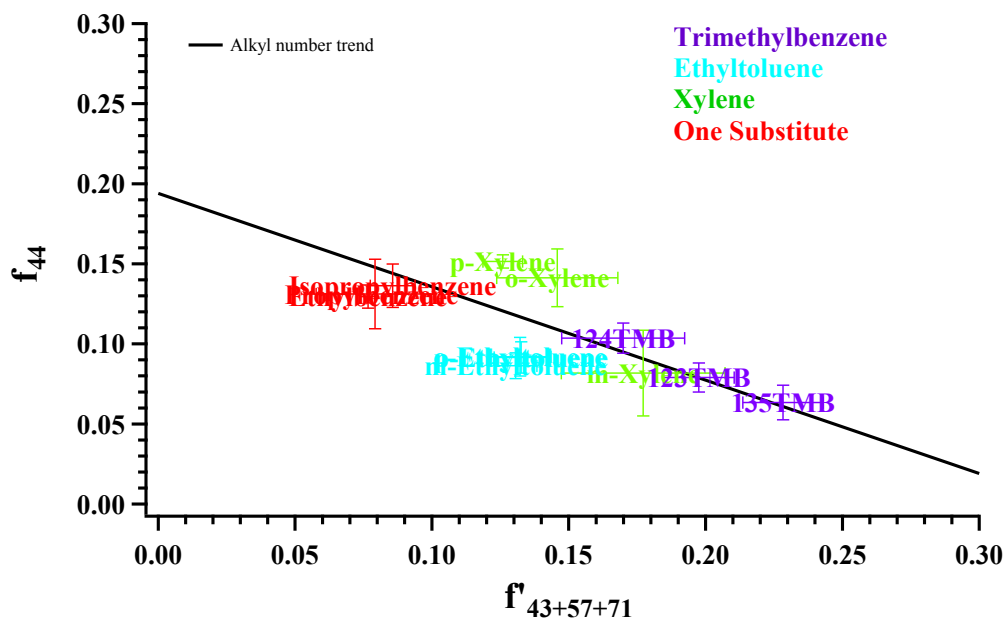
Fig. 2. f_{44+} vs. $f'_{43+57+71}$ in SOA formed from different aromatic hydrocarbon photooxidation under low NO_x colored by aromatic isomer type and marked with individual aromatic hydrocarbon species: Ethylbenzene 2084A; Propylbenzene 1245A; Isopropylbenzene 1247A; *m*-Xylene 1191A; *m*-Ethyltoluene 1199A; *o*-Xylene 1320A; *o*-Ethyltoluene 1179A; *p*-Xylene 1308A; *p*-Ethyltoluene 1194A; 1, 2, 3-Trimethylbenzene (123TMB) 1162A;1,2,4-Trimethylbenzene (124TMB) 1119A; 1, 3, 5-Trimethylbenzene (135TMB) 1156A. Alkyl number trend is the linear fitting in (Li., et al., 2015a) *Error bar stands for f_{44+} and $f'_{43+57+71}$ standard deviation when significant particles are formed (>5μg/m^3).
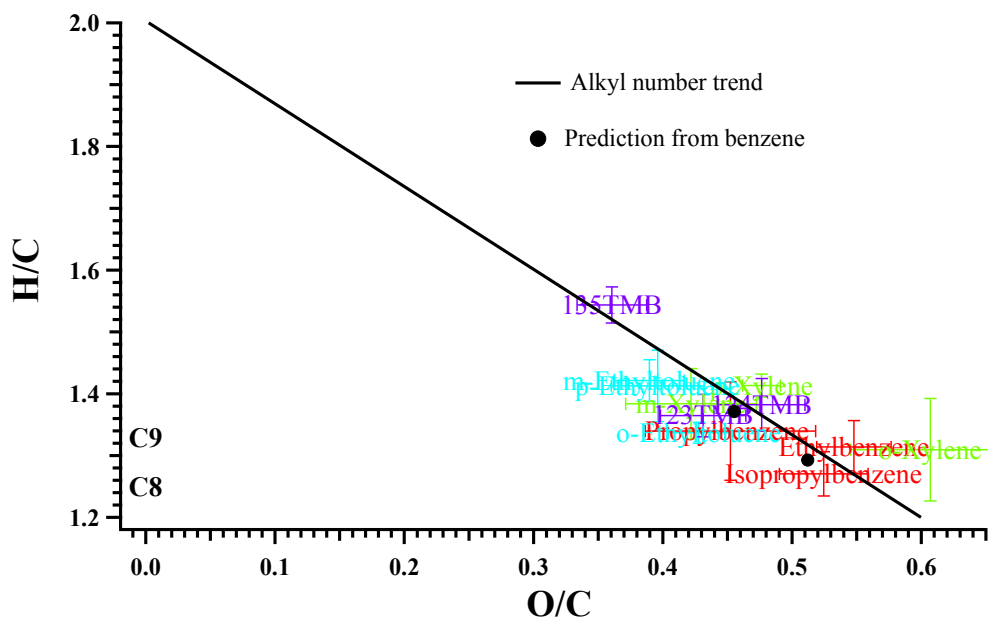
Fig. 3. H/C vs. O/C in SOA formed from different aromatic hydrocarbon photooxidation under low NO_x colored by aromatic isomer type and marked with individual aromatic hydrocarbon species (C8 and C9 on the lower left indicate the location of initial aromatic hydrocarbon precursor): Ethylbenzene 2084A; Propylbenzene 1245A; Isopropylbenzene 1247A; *m*-Xylene 1191A; *m*-Ethyltoluene 1199A; *o*-Xylene 1320A; *o*-Ethyltoluene 1179A; *p*-Xylene 1308A; *p*-Ethyltoluene 1194A; 1, 2, 3-Trimethylbenzene (123TMB) 1162A; 1, 2, 4-Trimethylbenzene(124TMB) 1119A; 1, 3, 5-Trimethylbenzene(135TMB) 1156A. Alkyl number trend is the linear fitting in (Li., et al., 2015a). Solid black cycles are SOA elemental ratio from C_8 and C_9 aromatic hydrocarbon predicted by SOA elemental ratio formed from benzene. *Error bar stands for H/C and O/C standard deviation when significant particles are formed ($>5\mu g/m^3$).
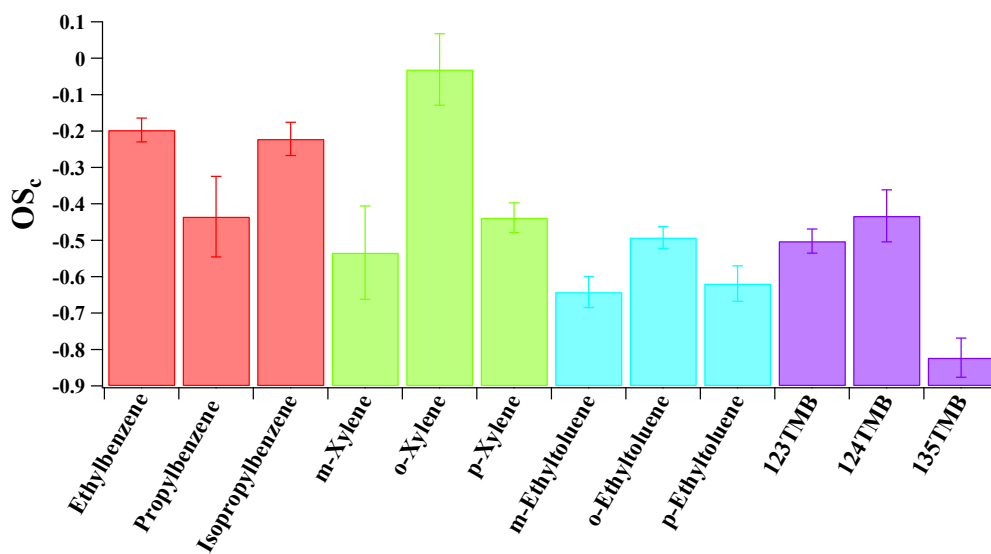
Fig. 4. Oxidation state (OS$_c$) of SOA formed from different aromatic hydrocarbon photooxidation under low NO$_x$: Ethylbenzene 2084A; Propylbenzene 1245A; Isopropylbenzene 1247A; *m*-Xylene 1191A; *m*-Ethyltoluene 1199A; *o*-Xylene 1320A; *o*-Ethyltoluene 1179A; *p*-Xylene 1308A; *p*-Ethyltoluene 1194A; 1, 2, 3-Trimethylbenzene (123TMB) 1162A; 1, 2, 4-Trimethylbenzene(124TMB) 1119A; 1, 3, 5-Trimethylbenzene(135TMB) 1156A.
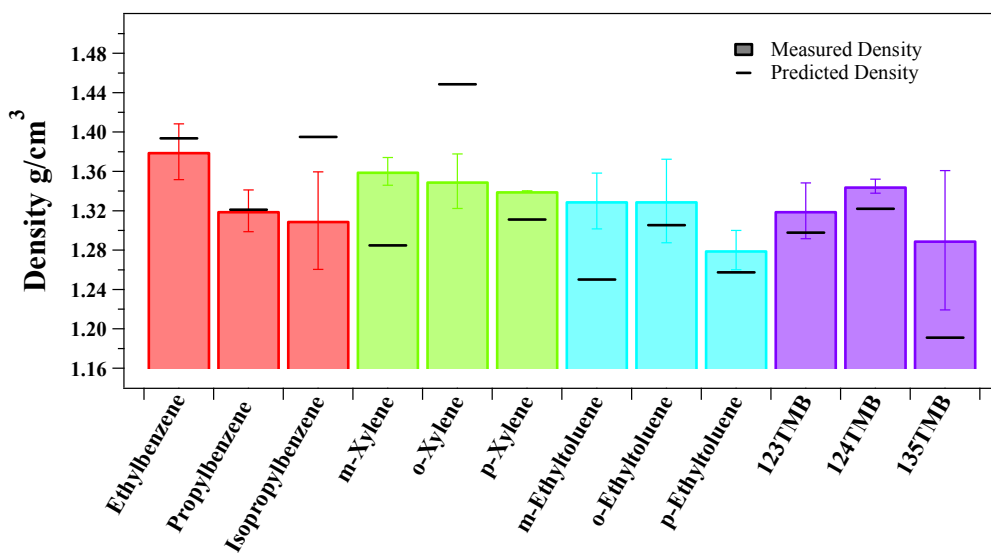
Fig. 5. Measured and predicted SOA density from different aromatic hydrocarbon photooxidation under low NO_x (Colored with substitute number and length, one substitute-red, xylenes-green, ethyltoluenes-blue and trimethylbenzene-purple; black line is predicted density according to Kuwata, et al., 2011); 123TMB- 1, 2, 3-Trimethylbenzene; 5   135TMB- 1, 3, 5-Trimethylbenzene; 124TMB- 1, 2, 4-Trimethylbenzene.
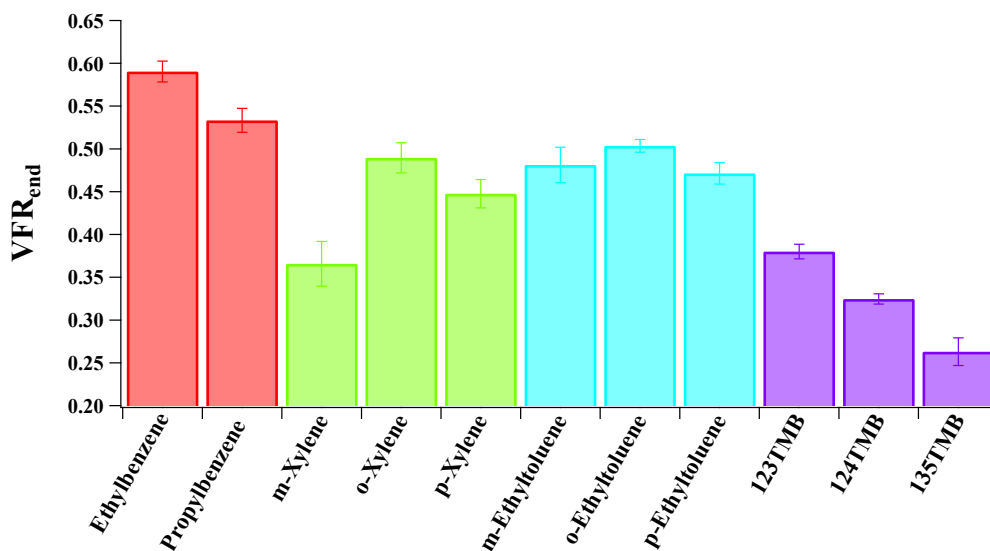
Fig. 6. SOA Volume fraction remaining (VFR_{end}) at the end of aromatic hydrocarbon photooxidation under low NO_x (Colored with substitute number and length, one 10   substitute-red, xylenes-green, ethyltoluenes-blue and trimethylbenzene-purple); 123TMB- 1, 2, 3-Trimethylbenzene; 135TMB- 1, 3, 5-Trimethylbenzene; 124TMB- 1, 2, 4-Trimethylbenzene.

(a)

(b)
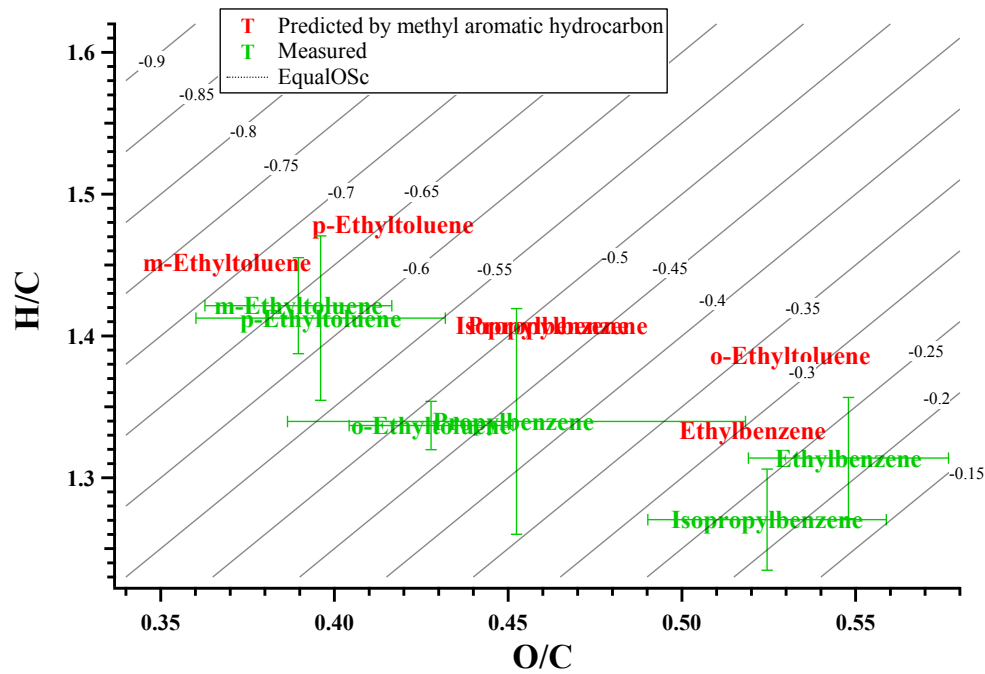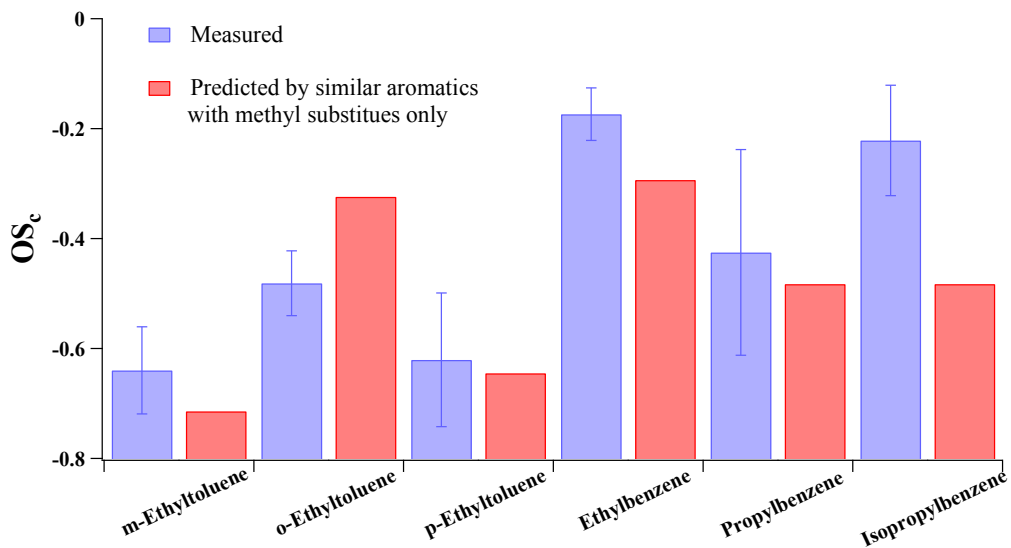
Fig. 7. Comparison of measured and predicted elemental ratio (a) and oxidation state (b) of SOA formed from longer alkyl substitute ($-C_2H_{2n+1}$, n>1). Ethyltoluenes are predicted by corresponding xylenes and one substitute aromatic hydrocarbons are predicted by toluene.*Predicted elemental ratio of isopropylbenzene is same as propylbenzene (not showed in Fig. a)

Radical conditions are important to SOA formation (Ng, et al., 2007; Li, et al., 2015) and $RO_2\cdot$ and $HO_2\cdot$ reaction is a major pathway to SOA formation (Kroll and Seinfeld, 2008;). The NO conditions used in this work assure that $RO_2\cdot$ and $HO_2\cdot$ reaction is a major pathway during the oxidation of the aromatic studies (Fig. S1). The relationship of SOA yield to a number of radical parameters were analyzed based the average radical parameters during photooxidation (Table S4). $[HO_2\cdot]$ shows a correlation (0.35~0.4) with yield when C_8 and C_9 aromatic hydrocarbons are analyzed either all together or individually. Fig S2 shows the relationship of $[HO_2\cdot]$ to yield. Fig S2 is colored by substitute number or position and sized with mass loading M_0. Particle size generally grows larger from left to right demonstrating a positive correlation with M_0 and $[HO_2\cdot]$ (0.43, p-value=0.00). A similar size circle in each vertical slice illustrates SOA yield differences between isomers at similar $[HO_2\cdot]$ condition. Two typical slices are boxed to compare isomer SOA yield. The left slice shows that one substitute isomers (turquoise) form more SOA than three substitute ones (mustard) at similar mass loading and radical concentrations. The right slice shows that ortho position isomers (purple) yields are higher than para ones (red). Additionally, a trend showing that ortho position isomers (purple) have higher yield than the meta isomers when $M_0>40$ µg·m^{-3}(larger size cycle) and $15-35*10^6$ molecules·cm^{-3} $[HO_2\cdot]$. Radical analysis in general further supports the relationship found between SOA yield and precursor molecular structure.

It is further noticed that the low $[HO_2\cdot]$ and yield correlation is due to the difference in isomer k_{OH} (Table S1). It is found that k_{OH} correlates well with yield especially when only C_9 isomers are considered (-0.451, p-value=0.002). The ~~reverse~~ inverse correlation explains that SOA yield hinges on molecular structure instead of kinetic reaction rate (Li, et al., 2016). The insignificant correlation between k_{OH} and C_8 isomers is due to a greater impact of molecular structure on SOA formation than k_{OH}.

Table S1 Aromatic hydrocarbon physical properties and rate constant

Compound	Vapor Pressure[a]	Boiling Point[b]	k_{OH}[c]
	mmHg	°C	$10^{-11} cm^3\ molecule^{-1}\ s^{-1}$
Ethylbenzene	9.2	136	0.70
Propylbenzene	3.1	159	0.58
Isopropylbenzene	4.5	152	0.63
m-Xylene	9.0	139	2.31
o-Xylene	6.0	144	1.36
p-Xylene	7.9	138	1.43
m-Ethyltoluene	3.0	158	1.86
o-Ethyltoluene	2.6	164	1.19
p-Ethyltoluene	2.9	162	1.18
1,2,4-Trimethylbenzene	2.1	170	3.25
1,2,3-Trimethylbenzene	1.4	175	3.27
1,3,5-Trimethylbenzene	2.3	165	5.67

Note: a) vapor pressures are referred to Chemispider at 25 °C; b) boiling points are referred to Chemispider; c) OH reaction rate constants used in SAPRC-11 model at 25 °C ;   *Predicted data from on Chemispider.

Table S2 Experiment conditions of additional aromatic hydrocarbon experiments

Precursor	ID	HC/NO	NO	HC	ΔHC	M_0	Yield
		ppbC:ppb	ppb	ppb	$\mu g \cdot m^{-3}$	$\mu g \cdot m^{-3}$	
m-xylene[1,3]	104A	10.1	64.4	81.3	328	21.7	0.07
	104B	29.3	21.4	78.4	281	20.4	0.07
	129A	15.1	45.5	86	336	21.9	0.07
	149A	13.3	50.2	83.6	342	52.8	0.15
	164A	12.4	44.0	68.0	271	16.8	0.06
	164B	12.2	44.1	67.5	270	14.6	0.05
	217A	36.8	8.90	40.9	155	9.80	0.06
	217B	35.9	8.70	39	153	7.90	0.05
	219A	63.7	7.00	55.7	165	9.20	0.06
	219B	67.5	6.60	55.7	166	9.30	0.06
	288A	63.1	7.00	55.2	183	9.00	0.05
	290A	31.1	15.3	59.5	229	9.00	0.04
	293A	29.9	13.7	51.2	189	9.20	0.05
	368A	17.9	21.0	47.0	149	6.90	0.05
	485A	17.5	43.3	94.7	353	37.2	0.11
	485B	16.7	45.0	93.7	349	40.4	0.12
	488A	15.5	46.2	89.6	341	29.5	0.09
	492A	13.6	44.3	75.2	296	29.1	0.10
	492B	13.5	44.8	75.5	298	29.7	0.10
	566A	14.0	48.3	84.5	337	48.2	0.14
	566B	13.3	48.0	79.8	318	48.4	0.15
	758A	47.5	11.4	67.7	158	13.5	0.09
	820A	30.2	20.7	78.1	260	17.0	0.07
	1193A	15.5	36.8	71.1	239	13.6	0.06
	1193B	15.2	36.5	69.5	236	11.2	0.05
	1191A	12.6	52.2	82.1	298	15.2	0.05
	1191B	14.6	45.7	83.6	340	14.6	0.04
	1516A	27.8	26.7	92.9	357	48.7	0.14
	1950A	14.1	45.5	80.0	327	26.3	0.08
	1950B	14.6	45.9	83.6	345	28.7	0.08
o-xylene[2]	503B	15.5	75.0	145	448	30.0	0.07
	505A	171	48.0	1026	360	32.0	0.09
	508A	17.9	24.3	54.3	208	12.5	0.06
	517B	30.9	26.8	103.7	296	32.0	0.11
	522A	8.80	52.0	57.1	220	7.70	0.04
	522B	41.7	11.0	57.4	171	15.0	0.09
p-xylene[2]	422B	33.1	23.9	98.8	211	5.90	0.03
	502A	41.0	21.0	108	292	19.0	0.07
	503A	18.0	75.0	169	579	66.0	0.11
	504A	16.3	129	263	876	103	0.12
	504B	15.8	131	260	675	52.0	0.08
	515B	18.5	26.0	60.3	200	8.00	0.04
	519B	29.2	53.0	194	450	36.5	0.08
	525A	45.3	10.2	57.8	163	8.0	0.05
1, 2, 4-	1117A	69.8	10.3	80.0	335	16.8	0.05

trimethylbenzene	1117B	34.8	20.7	80.0	368	18.2	0.05
	1119A	14.1	49.8	78.0	385	19.6	0.05
	1119B	17.1	41.6	79.0	390	25.5	0.07
	1123A	71.0	10.1	80.0	300	11.2	0.04
	1123B	32.6	22.1	80.0	345	15.4	0.05
	1126A	69.3	10.1	77.5	286	12.6	0.04
	1126B	28.1	24.3	75.9	333	15.4	0.05
	1129B	24.2	15.6	42.0	201	5.60	0.03

Table S3. Two product yield curve fitting parameters for selected compounds

Yield Curve	α_1	$K_{om,1}$ $(m^3 \cdot \mu g^{-1})$	α_2	$K_{om,2}$ $(m^3 \cdot \mu g^{-1})$
Ethylbenzene	0.160	0.039	0.138	0.005
Propylbenzene (i- and n-)	0.117	0.040	0.139	0.005
o-Xylene	0.141	0.025	0.264	0.005
o-Ethyltoluene	0.173	0.024	0.247	0.005
m-Xylene	0.166	0.036	0.083	0.005
m-Ethyltoluene	0.152	0.036	0.085	0.005
p-Xylene	0.168	0.026	0.016	0.005
p-Ethyltoluene	0.144	0.022	0.049	0.005

Table S4 Average radical concentrations during photooxidation

Run ID	RO$_2$[a]	HO$_2$[a]	OH[b]	HO$_2$*RO[c]	HO$_2$/RO$_2$	NO/HO$_2$	OH/HO$_2$[d]	NO$_3$[a]
1142A	17.0	13.78	9.21	474	1.50	4.0E+04	1.5E-01	9.60
1142B	1.38	3.08	5.61	12.6	2.16	3.6E+05	4.8E-01	15.9
1146A	11.3	14.07	4.52	225	1.60	6.9E+02	2.0E-02	4.21
1146B	14.8	14.68	6.91	340	1.42	6.0E+03	5.0E-02	5.92
2084A	12.5	16.99	1.91	257	1.60	1.2E+02	3.7E-03	1.62
2084B	10.1	15.07	1.62	189	1.72	1.4E+02	3.7E-03	1.36
1245A	8.22	10.66	4.17	132	1.49	2.3E+03	3.0E-02	4.75
1246A	8.71	9.03	4.28	194	1.55	2.1E+05	2.3E-01	24.8
1247A	15.6	15.48	5.21	338	1.38	7.6E+02	2.0E-02	3.04
1247B	11.2	10.99	7.56	280	1.62	2.5E+07	2.3E+01	9.12
1253A	23.7	20.12	6.47	726	1.23	2.1E+05	4.3E-01	5.18
1253B	4.24	6.74	5.02	100	2.00	1.1E+05	1.6E-01	28.4
1193A	11.0	12.33	3.14	185	1.34	1.5E+06	1.8E+00	14.0
1193B	8.97	11.59	2.82	141	1.44	3.2E+05	4.2E-01	18.7
1191A	19.1	15.83	5.81	449	1.23	4.5E+05	3.4E-01	32.1
1191B	10.8	12.43	2.36	189	1.46	3.8E+04	5.1E-02	18.5
1516A	18.6	23.1	3.14	465	1.33	1.5E+01	2.0E-03	2.37
1950A	11.7	20.62	4.46	267	1.84	7.2E+01	4.3E-03	38.4
1950B	13.3	22.03	4.64	326	1.74	4.6E+01	3.7E-03	37.1
1315A	17.5	20.7	8.28	495	1.52	1.0E+03	1.8E-02	28.9
1315B	19.8	21.59	5.20	478	1.23	3.5E+01	4.3E-03	3.38
1320A	53.2	21.02	11.9	1432	0.79	3.7E+02	1.7E-02	1.77
1321A	21.0	21.35	5.14	506	1.20	3.1E+01	4.1E-03	2.46
1321B	22.9	19.43	3.58	484	1.02	4.3E+00	2.1E-03	0.72
1308A	12.5	13.89	7.04	308	1.40	2.0E+05	3.9E-01	15.9
1308B	24.0	18.01	5.66	564	1.00	1.0E+03	1.6E-02	3.36
1151A	8.97	14.15	9.27	251	0.00	2.4E+04	8.0E-02	66.7
1151B	23.3	22.14	9.83	788	1.40	5.6E+03	3.6E-02	13.3
1199A	15.1	22.49	4.16	373	1.57	8.1E+01	4.0E-03	24.0
1222B	20.3	27.24	8.11	625	1.15	9.7E+01	4.1E-03	55.5
1226B	24.3	32.15	5.66	885	1.44	3.2E+02	5.8E-03	105
1232A	22.2	30.55	4.57	774	1.52	2.3E+02	4.4E-03	104
1421A	20.0	22.36	3.05	504	1.30	3.7E+00	1.5E-03	2.43
1421B	23.2	27.06	6.33	710	1.30	2.3E+01	3.6E-03	13.7
1179A	12.6	17.6	5.26	294	1.72	3.9E+02	1.0E-02	51.5
1179B	14.0	19.05	5.50	329	1.60	2.2E+02	8.2E-03	51.1
1202A	13.8	17.77	5.94	350	1.57	8.5E+03	3.9E-02	39.6
1215A	25.7	25.73	6.06	981	1.47	3.3E+03	1.8E-02	53.1
1413A	19.1	20.64	3.54	430	1.17	1.7E+01	2.6E-03	3.00
1413B	20.9	22.76	6.96	550	1.24	2.1E+02	8.7E-03	19.4
1194A	23.1	20.6	3.85	675	1.16	5.1E+04	5.9E-02	37.4
1194B	23.5	20.04	4.10	712	1.19	3.9E+04	5.3E-02	26.4
1197A	25.2	20.97	3.60	733	1.13	1.8E+04	4.0E-02	5.61
1197B	24.6	19.92	5.18	782	1.04	1.0E+08	3.7E+01	20.5
1214B	22.3	18.34	7.57	623	1.16	6.4E+03	4.3E-02	14.4
1601A	36.8	31.89	9.25	1489	0.99	9.7E+06	2.1E+01	6.21
1158A	20.1	18.64	1.68	391	1.04	4.2E+00	1.0E-03	1.35
1158B	43.4	21.98	3.49	957	0.72	2.9E-01	1.6E-03	1.28
1162A	19.7	23.94	4.75	523	1.42	7.9E+00	2.4E-03	37.2
1162B	96.9	19.22	5.78	1445	0.44	3.8E-02	3.5E-03	0.33

1117A	13.1	15.79	1.69	220	1.29	1.2E+01	1.5E-03	7.29
1117B	9.83	14.58	2.49	172	1.58	1.9E+02	4.7E-03	34.9
1119A	12.5	18.77	5.29	300	1.66	2.7E+03	1.7E-02	89.0
1119B	12.1	17.26	3.95	296	1.86	2.9E+03	1.7E-02	68.7
1123A	15.9	15.09	1.66	274	1.06	6.8E+01	2.2E-03	2.91
1123B	15.8	18.56	2.54	321	1.22	7.7E+01	3.0E-03	23.2
1126A	17.3	17.63	1.69	324	1.07	1.7E+01	1.5E-03	4.26
1126B	29.9	24.76	7.50	841	1.03	3.2E+01	3.8E-03	33.7
1129B	11.2	15.45	4.29	199	1.58	5.6E+01	4.9E-03	24.0
1153A	14.9	18.64	1.10	292	1.28	1.2E+01	8.3E-04	1.22
1153B	17.5	21.78	1.99	411	0.00	1.6E+01	1.3E-03	3.33
1156A	11.1	19.85	2.08	249	1.97	2.5E+01	1.6E-03	31.8
1156B	9.86	19.63	2.85	218	2.18	6.1E+01	2.8E-03	54.4
1329B	2.51	9.07	4.45	26.0	4.62	2.2E+02	8.0E-03	125

Note: average radical concentrations are calculated by dividing time integrated radical parameters with photooxidation time; average radical concentration throughout photooxidation a) in 10^6 molecules·cm^{-3}; b) in 10^8 molecules·cm^{-3}; c) in 10^{16} molecules·cm^{-3}; d) average radical ratio throughout photooxidation in 10^3

Table S5 Correlation between SOA yields and average radical concentrations

C_8 & C_9	RO_2	HO_2	OH	HO_2*RO_2	HO_2/RO_2	NO/HO_2	OH/HO_2	NO_3
Yield	0.152	0.393	-0.046	0.24	-0.099	-0.046	-0.108	0.093
p-value[a]	0.223	0.001	0.714	0.053	0.428	0.712	0.388	0.457

C_9	RO_2	HO_2	OH	HO_2*RO_2	HO_2/RO_2	NO/HO_2	OH/HO_2	NO_3
Yield	0.189	0.376	0.098	0.303	-0.133	-0.07	-0.141	0.094
p-value[a]	0.208	0.010	0.516	0.040	0.380	0.644	0.349	0.535

C_8	RO_2	HO_2	OH	HO_2*RO_2	HO_2/RO_2	NO/HO_2	OH/HO_2	NO_3
Yield	-0.092	0.353	-0.386	-0.094	0.200	-0.293	-0.318	-0.278
p-value[a]	0.699	0.127	0.093	0.693	0.398	0.209	0.171	0.235

Note: C_8 & C_9 correlation analysis used all the experiments listed in Table S4, C_8 or C_9 correlation analysis only used C_8 or C_9 isomer experiments listed in Table S4. a) P-values range from 0 to 1, 0-reject null hypothesis and 1 accept null hypothesis. Alpha (α) level used is 0.05. If the p-value of a test statistic is less than alpha, the null hypothesis is rejected

Table S6. SOA Fragments in HR-TOF-AMS at m/z 43, 57 and 71*

Compound	m/z					
	43		44	57		71
	$C_2H_3O^+$	$C_3H_7^+$	CO_2^+	$C_3H_5O^+$	$C_4H_9^+$	$C_4H_7O^+$
Ethylbenzene	×		×	×		
Propylbenzene	×	×	×	×	×	×
Isopropylbenzene	×	×	×	×		×
m-Xylene	×		×			
m-Ethyltoluene	×		×	×		
o-Xylene	×		×			
o-Ethyltoluene	×		×	×		
p-Xylene	×		×			
p-Ethyltoluene	×		×	×		
1,2,3-Trimethylbenzene	×		×	×		
1,2,4-Trimethylbenzene	×			×		
1,3,5-Trimethylbenzene	×		×	×		

* Experimental runs same as Fig. S4.
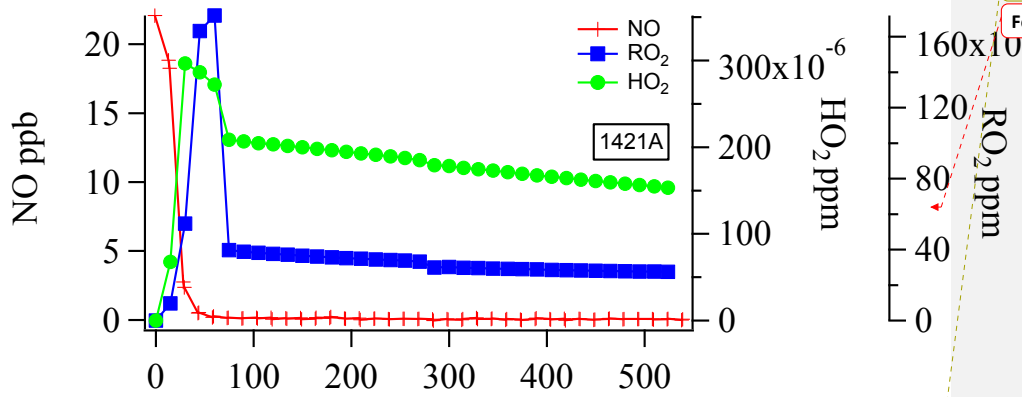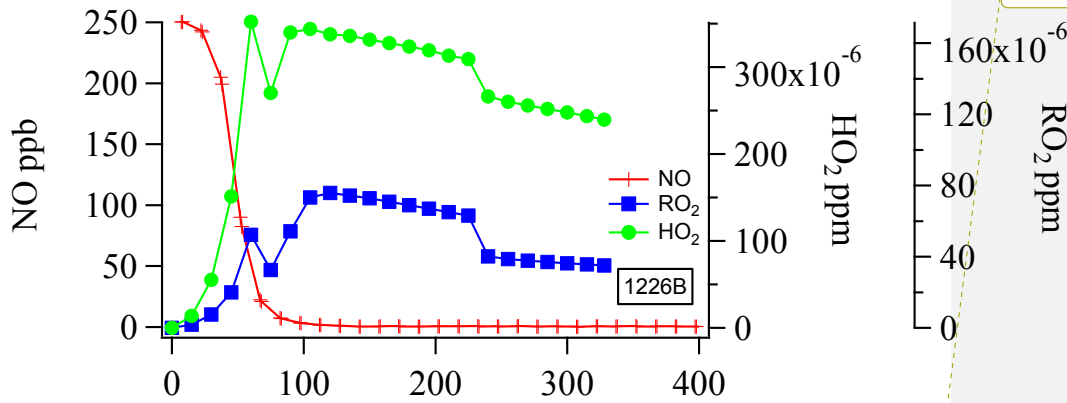
(a)

(b)

Fig. S1 Time series concentration change of NO, $HO_2 \cdot$ and $RO_2 \cdot$ during the phototoxidation of aromatic hydrocarbons. (m-Ethyltoluene, 1226B and 1421A; radical concentrations are predicted by SAPRC-11)
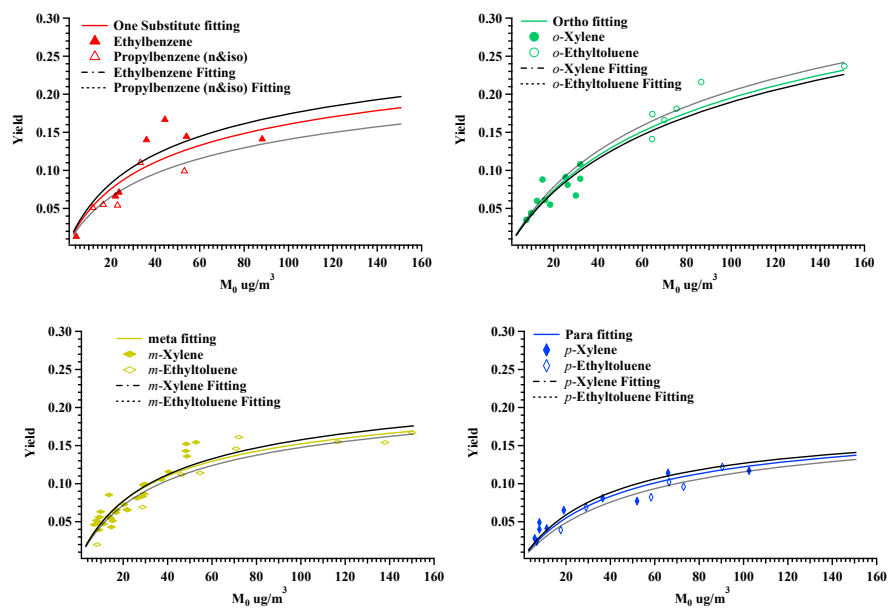
Fig. S1 S2. Aromatic SOA yields as a function of M_0 for single compounds: a) Ethylbenzene (dotted line) vs Propylbenzene (i- and n-)(dashed line); b) o-Xylene(dotted line) vs o-Ethyltoluene(dashed line); c) m-Xylene(dotted line) vs m-Ethyltoluene(dashed line); d) p-Xylene (dotted line) vs p-Ethyltoluene (dashed line) (Note: Song, et al, 2005; Song, et al, 2007; Li, et al., 2016 data are also included)
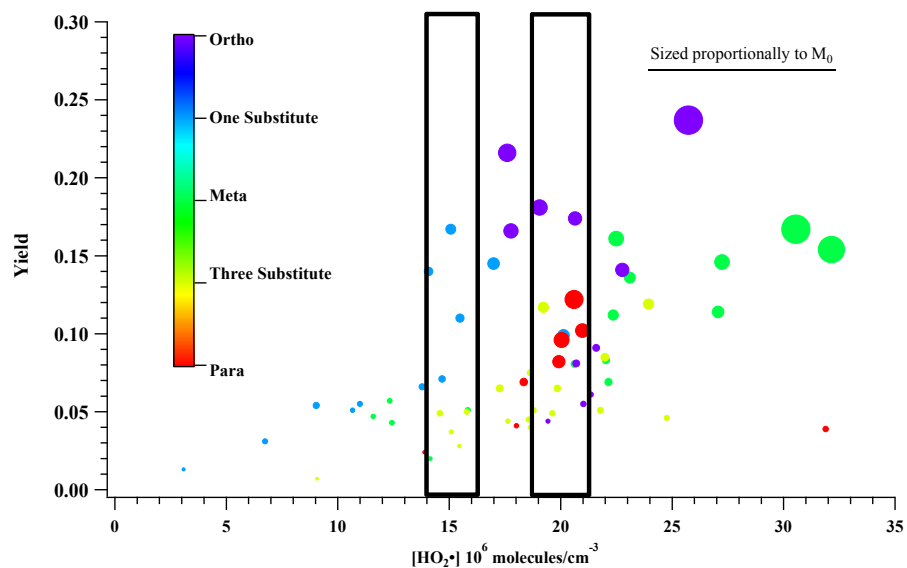
Fig. ~~S2~~ S3 Relationship between SOA yield and HO₂· radical concentration (Colored with substitute number or position and sized with mass loading M_0)
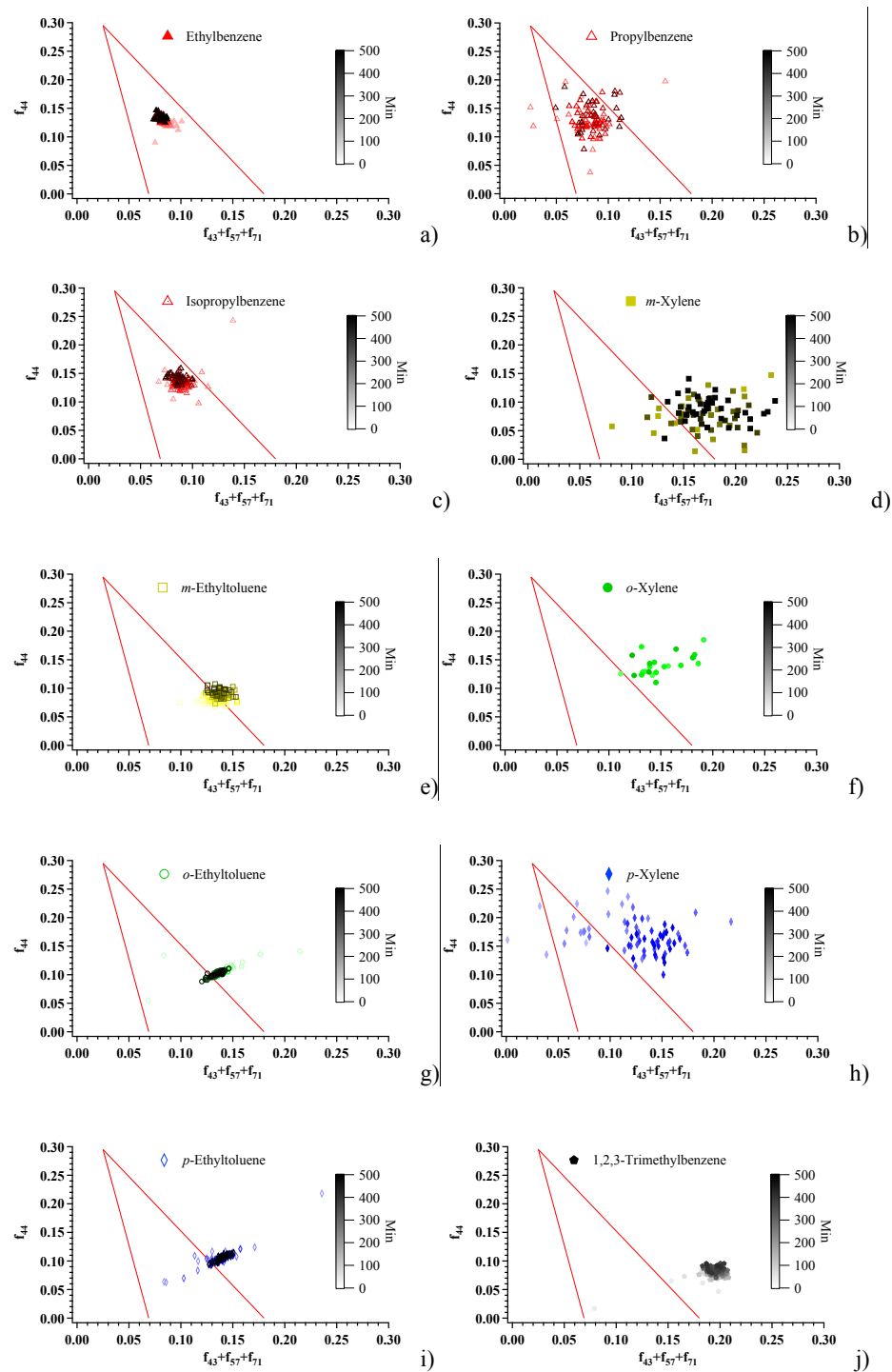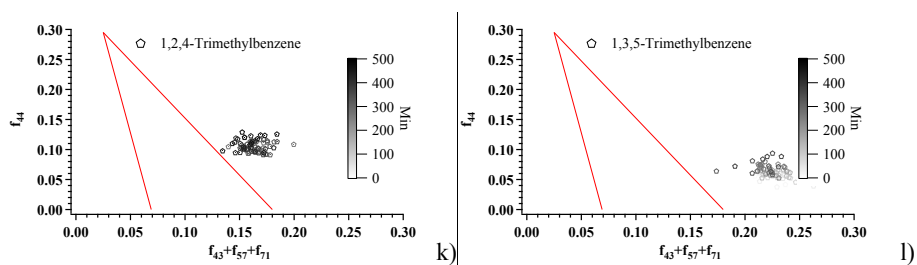
Fig. ~~S3~~ S4 f_{44} and $f_{43+57+71}$ evolution in SOA formed from different aromatic hydrocarbon photooxidation under low NO_x; each marker type represents one aromatic hydrocarbon and marker is colored with photooxidation time from light to dark: a) Ethylbenzene 2048A; b) Propylbenzene 1245A; c) Isopropylbenzene 1247A; d) *m*-Xylene 1191A; e) *m*-Ethyltoluene 1199A; f) *o*-Xylene 1320A; g) *o*-Ethyltoluene 1179A; h) *p*-Xylene 1308A; i) *p*-Ethyltoluene 1194A; j) 1,2,3-Trimethylbenzene 1162A; k) 1,2,4-Trimethylbenzene 1119A; l) 1,3,5-Trimethylbenzene 1156A

Diff, Hz/ns

C_2H_3O

2.0
1.5
1.0
0.5
0.0

42.9   43.1   43.2

a-1)

Diff, Hz/ns

CO_2

12
8
4
0

43.9   44.1   44.2

a-2)

Diff, Hz/ns

C_3H_5O

0.8
0.4
0.0

56.85 56.90 56.95 57.00 57.05 57.10 57.15 57.20

a-3)

Diff, Hz

C_2H_3O C_3H_7

0.8
0.6
0.0

42.9   43.0   43.1   43.2 b-1)

Diff, Hz

CO_2

6
4
2
0

43.9   44.0   44.1   44.2 b-2)

Diff, Hz

C_3H_5O C_4H_9

0.20
0.15
0.10
0.05
0.00
-0.05

56.85 56.90 56.95 57.00 57.05 57.10 57.15 57.20 b-3)
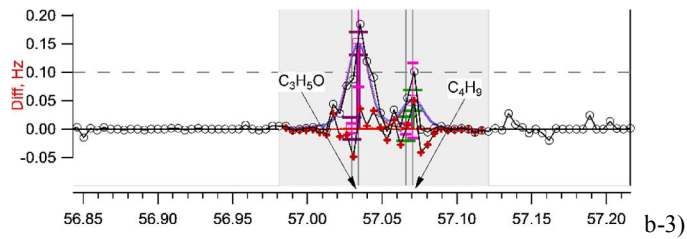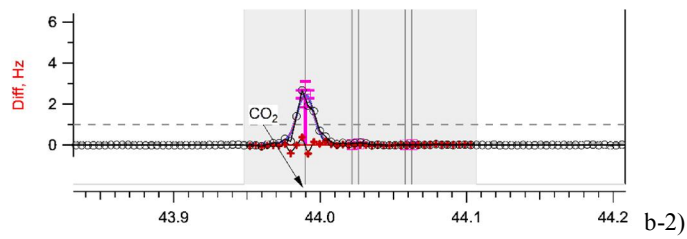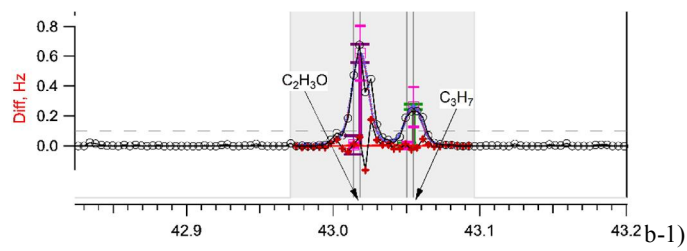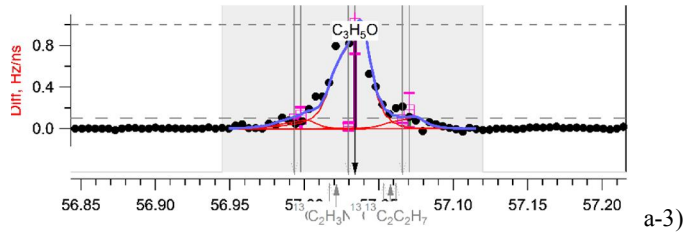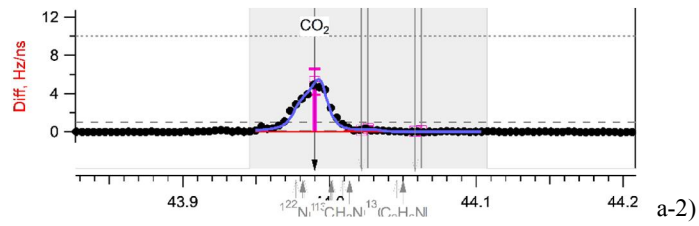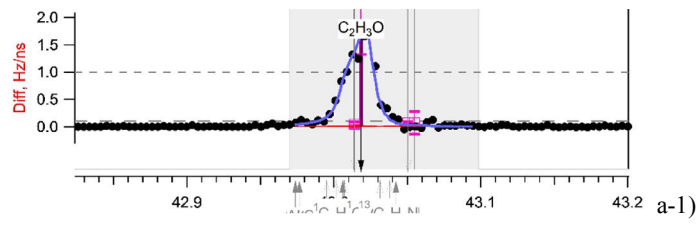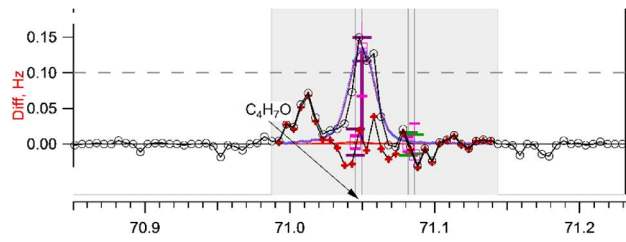
b-4)
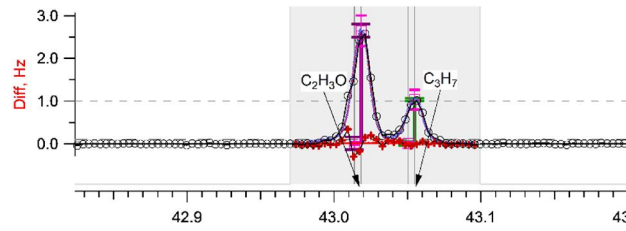
c-1)
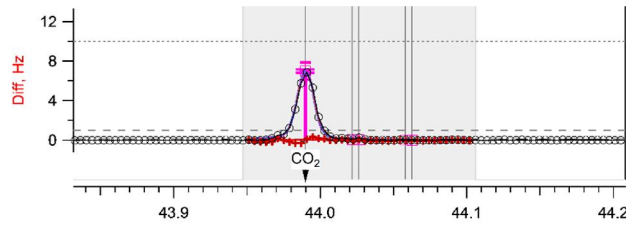
c-2)
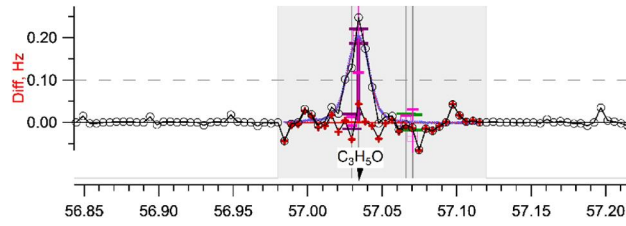
c-3)
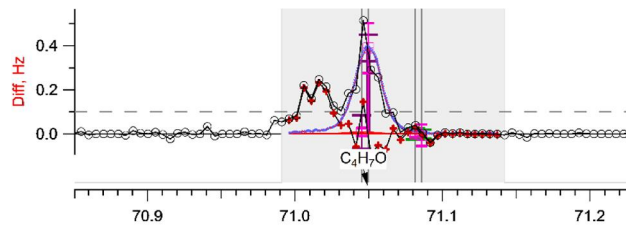
c-4)

d-1)

d-2)

e-1)

e-2)

e-3)

f-1)

f-2)

g-1)

g-2)

g-3)

h-1)

h-2)

i-1)

i-2)

i-3)

j-1)

j-2)

j-3)

k-1)

k-2)

l-1)

l-2)
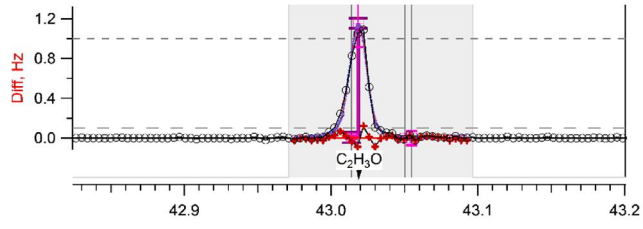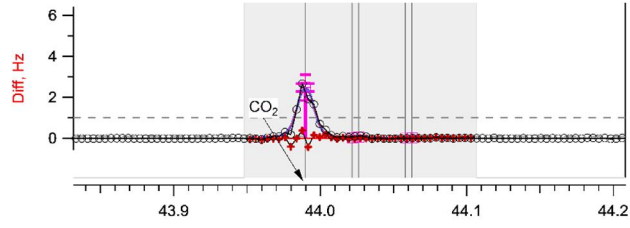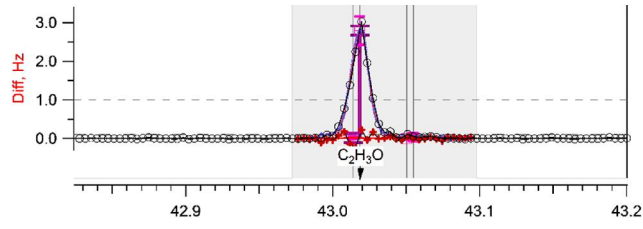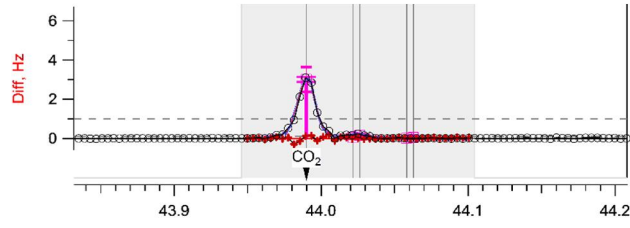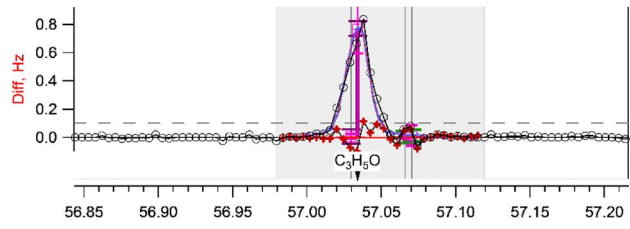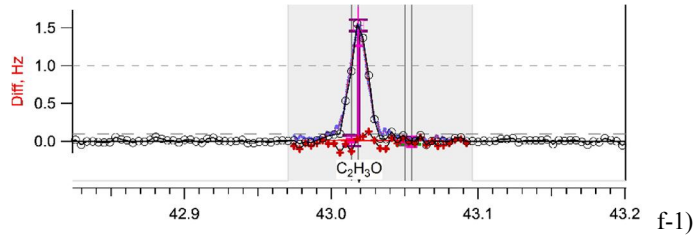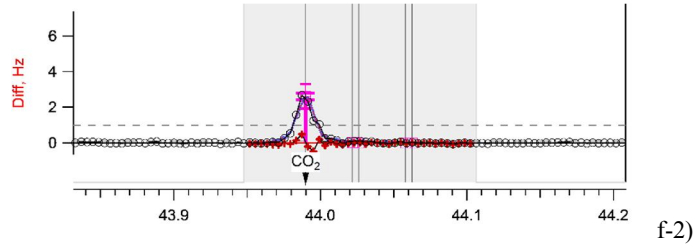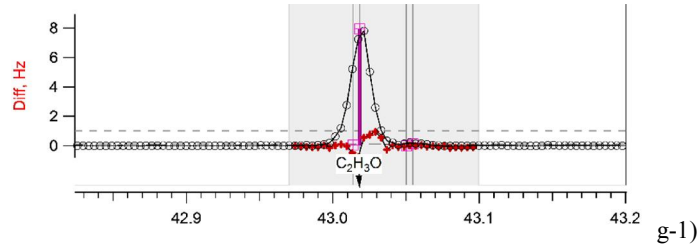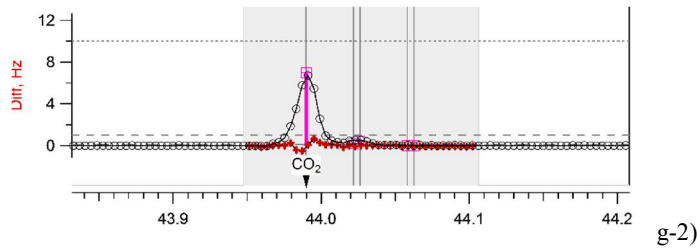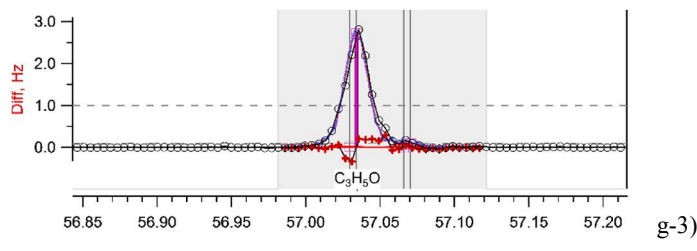
l-3)
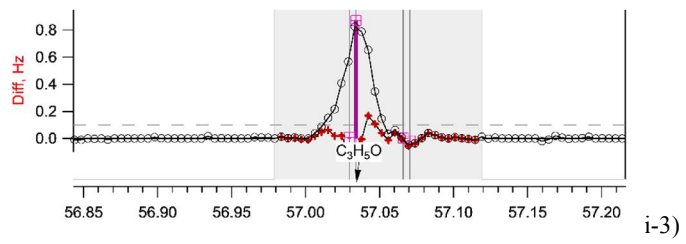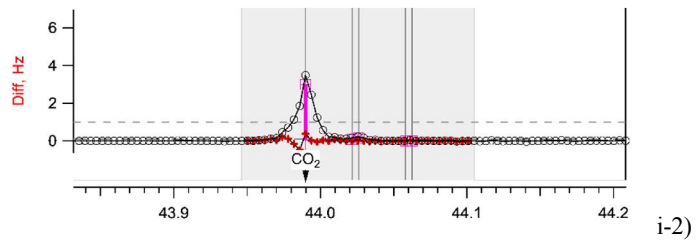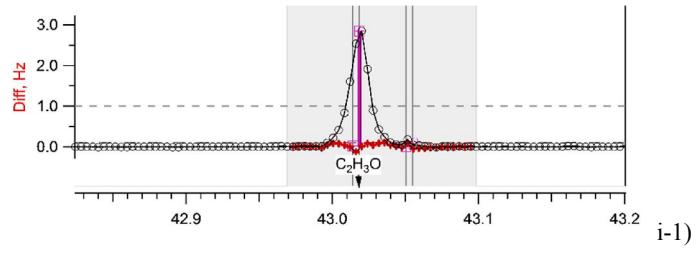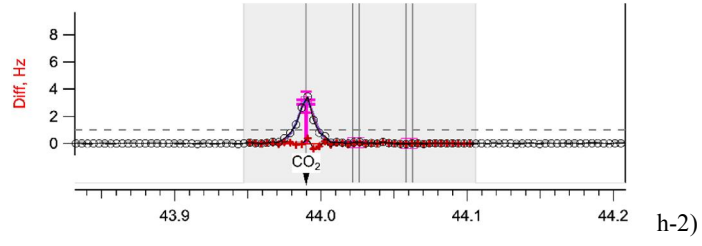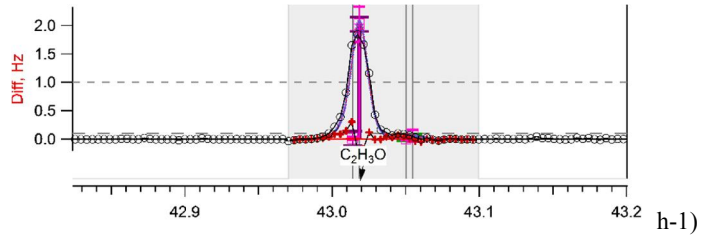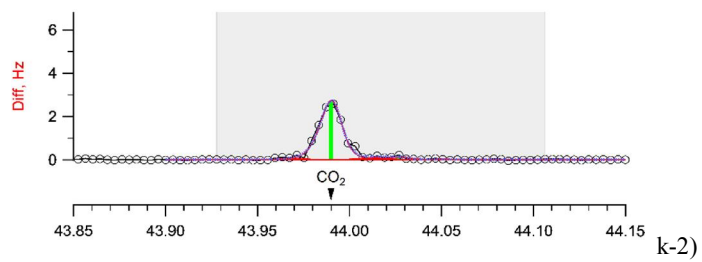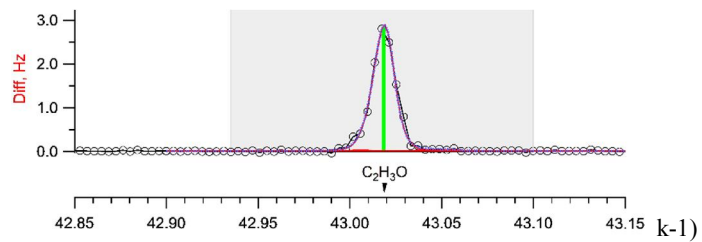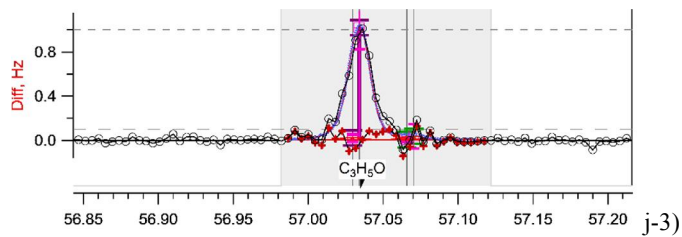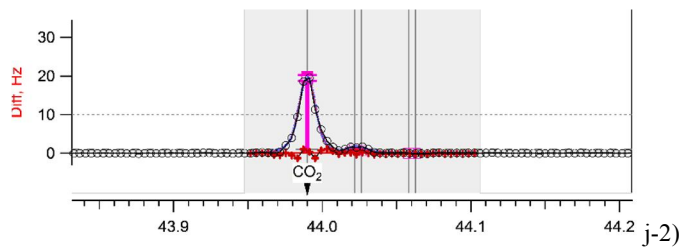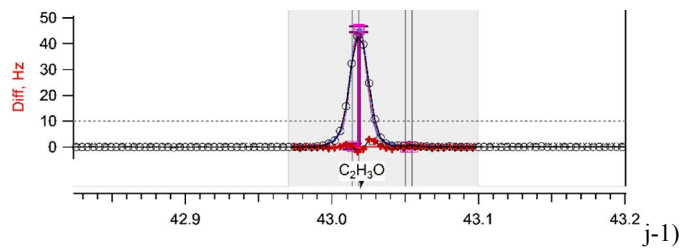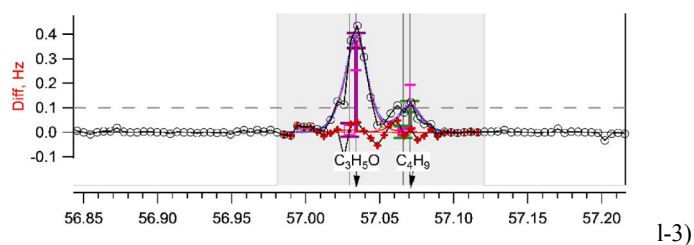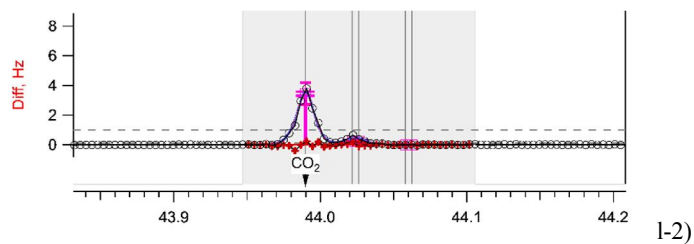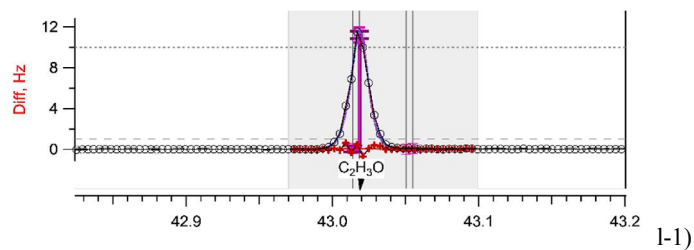
Fig. S4 S5 High-resolution mass spectra of m/z 43, m/z 44, m/z 57 and m/z 71 measured for secondary organic aerosol formed at peak aerosol concentration during aromatic photooxidation a) Ethylbenzene 1146A; b) Propylbenzene 1245A; c) Isopropylbenzene 1247A; d) *m*-Xylene 1191A; e) *m*-Ethyltoluene 1199A; f) *o*-Xylene 1320A; g) *o*-Ethyltoluene 1179A; h) *p*-Xylene 1308A; i) *p*-Ethyltoluene 1194A; j) 1,2,3-Trimethylbenzene 1162A; k) 1,2,4-Trimethylbenzene 1119A; l) 1,3,5-Trimethylbenzene 1156A (m/z 57 only includes $C_3H_5O^+$). *m/z peaks with intensity less than 0.1 are not displayed
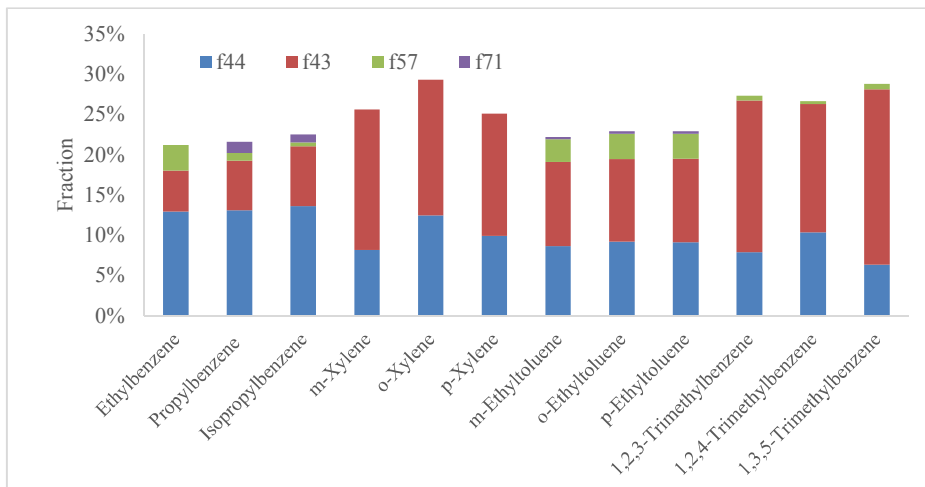
Fig. ~~S5~~ S6 m/z 43, m/z 44, m/z 57 and m/z 71 fraction in SOA formed from aromatic hydrocarbon photooxidation
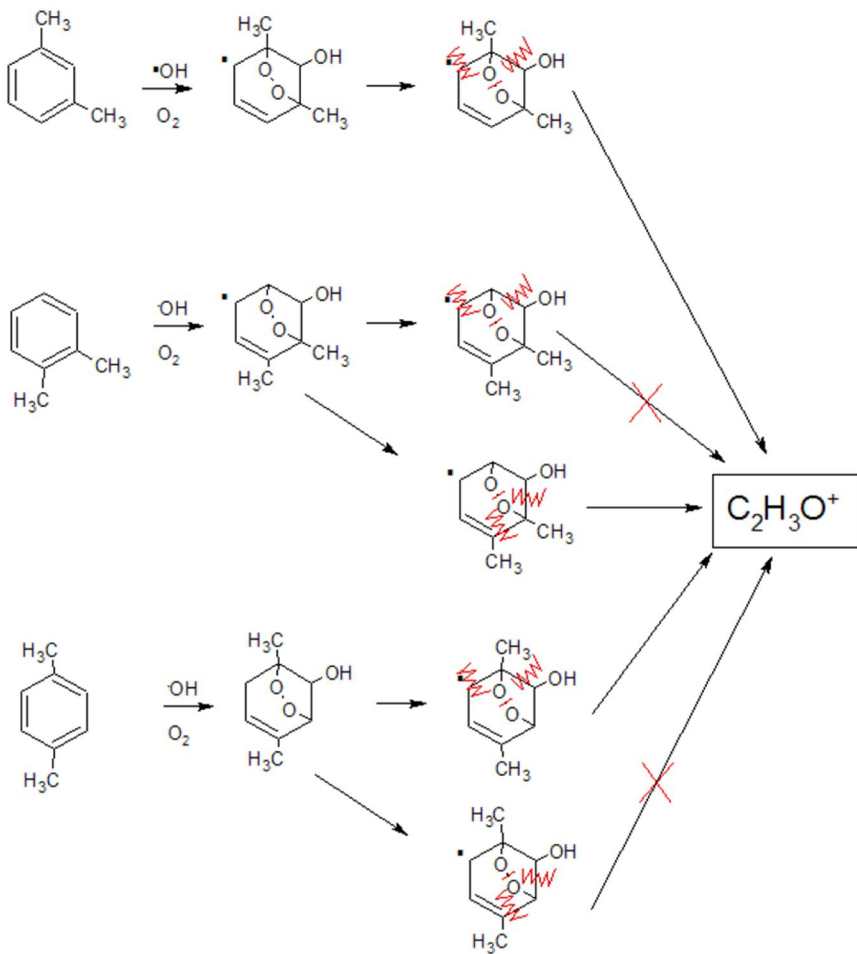
* Oxidation products of the bicyclic radicals lead to the formation of $C_2H_3O^+$. The bicyclic radicals show the origin of $C_2H_3O^+$ during the oxidation of aromatic hydrocarbons.

Fig. S6 S7 The potential relationship between alkyl substitute location and the $C_2H_3O^+$ fragments from HR-TOF-AMS.
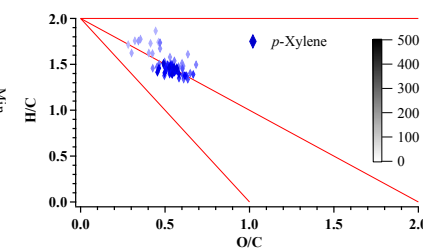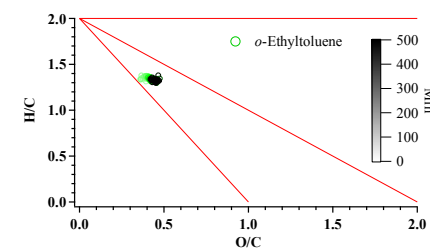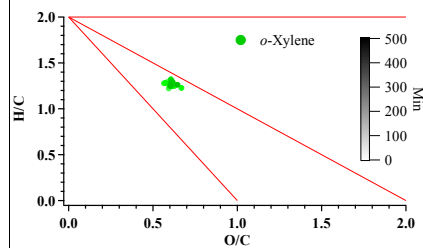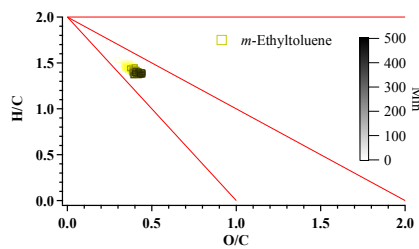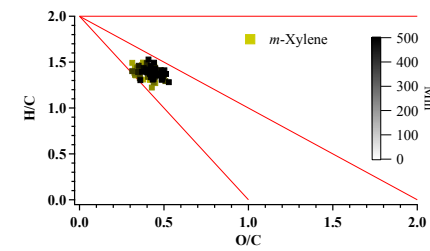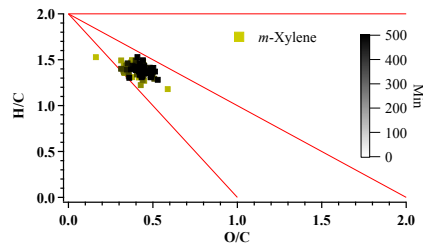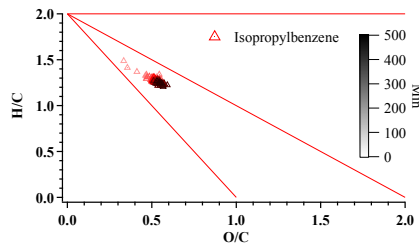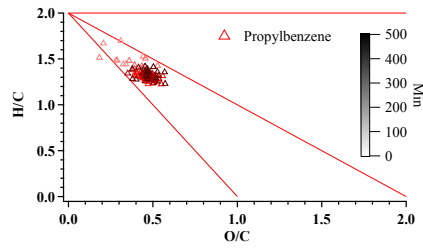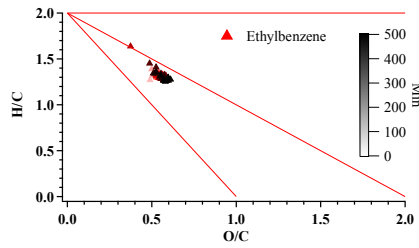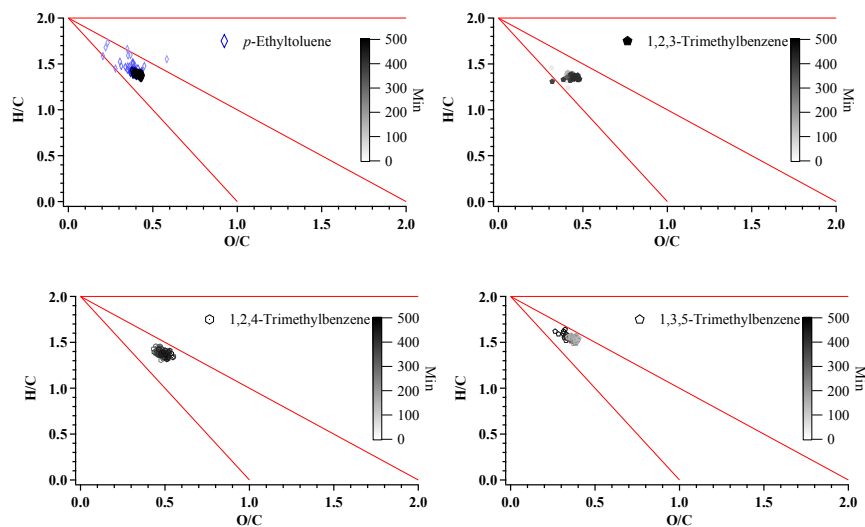
Fig. S7 S8 H/C and O/C evolution in SOA formed from different aromatic hydrocarbon photooxidation under low NO_x; each marker type represents one aromatic hydrocarbon and marker is colored with photooxidation time from light to dark: a) Ethylbenzene 1146A; b) Propylbenzene 1245A; c) Isopropylbenzene 1247A; d) *m*-Xylene 1191A; e) *m*-Ethyltoluene 1199A; f) *o*-Xylene 1320A; g) *o*-Ethyltoluene 1179A; h) *p*-Xylene 1308A; i) *p*-Ethyltoluene 1194A; j) 1, 2, 3-Trimethylbenzene 1162A; k) 1, 2, 4-Trimethylbenzene 1119A; l) 1, 3, 5-Trimethylbenzene 1156A.
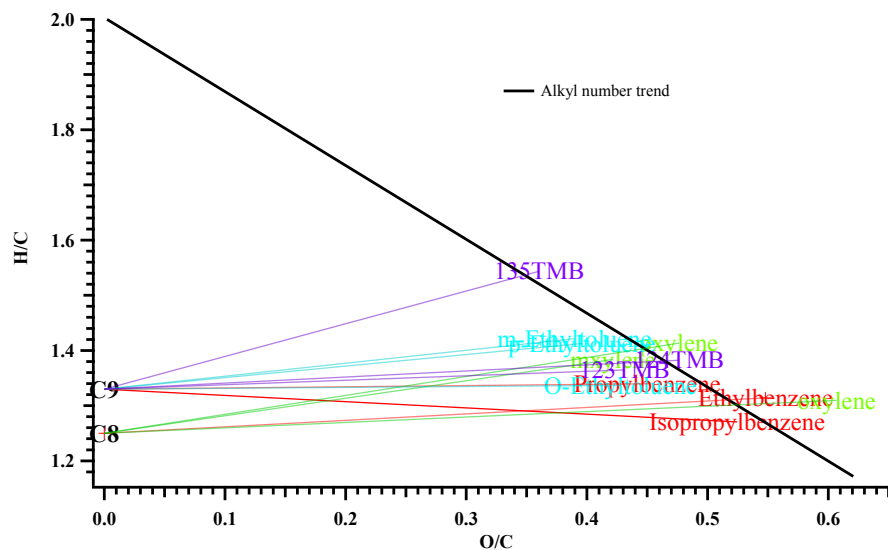
Fig. ~~S8~~ S9 H/C vs. O/C in SOA formed from different aromatic hydrocarbon photooxidation under low NO_x colored by aromatic isomer type and marked with individual aromatic hydrocarbon species (C8 and C9 on the lower left indicate the location of initial aromatic hydrocarbon precursor; dashed/solid line indicate that changes between precursor and SOA components): Ethylbenzene 2084A; Propylbenzene 1245A; Isopropylbenzene 1247A; *m*-Xylene 1191A; *m*-Ethyltoluene 1199A; *o*-Xylene 1320A; *o*-Ethyltoluene 1179A; *p*-Xylene 1308A; *p*-Ethyltoluene 1194A; 1, 2, 3-Trimethylbenzene (123TMB) 1162A;1, 2, 4-Trimethylbenzene(124TMB) 1119A; 1, 3, 5-Trimethylbenzene(135TMB) 1156A. Alkyl number trend is the liner fitting in (Li., et al., 2015a).
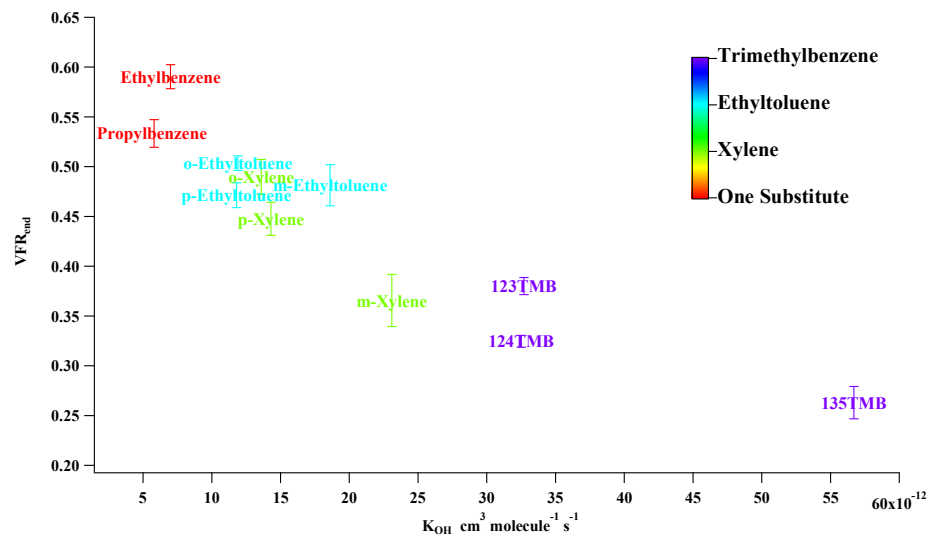
Fig S9 S10 Relationship between VFR and K_{OH} during aromatic hydrocarbon photooxidation under low NO_x